IEEE Access
Multidisciplinary ⋮ Rapid Review ⋮ Open Access Journal

Received September 3, 2020, accepted September 13, 2020, date of publication September 24, 2020,
date of current version October 6, 2020.

Digital Object Identifier 10.1109/ACCESS.2020.3026452

An Efficient Retrieval System for Biomedical Images Based on Radial Associated Laguerre Moments

GABER HASSAN[1], KHALID M. HOSNY[2], (Senior Member, IEEE), RUSHDY MOHAMED FAROUK[3], AND AHMED MANSOUR ALZOHAIRY[4]

[1]Department of Basic Sciences, Faculty of Engineering, Sinai University, North Sinai 45511, Egypt
[2]Department of Information Technology, Faculty of Computers and Informatics, Zagazig University, Zagazig 44511, Egypt
[3]Department of Mathematics, Faculty of Sciences, Zagazig University, Zagazig 44511, Egypt
[4]Genetics Department, Faculty of Agriculture, Zagazig University, Zagazig 44511, Egypt

Corresponding author: Gaber Hassan (gh_mcs86@yahoo.com)

The work of Ahmed Mansour Alzohairy was supported by the project H3ABioNet under Grant U24HG006941.

ABSTRACT The ability of any retrieval system to extract features by using its feature descriptor is the primary criterion to measure its efficiency. In this paper a novel technique for feature extraction of biomedical images is presented. The mooted system uses the Radial Associated Laguerre Moments (RALMs) as a feature descriptor to obtain features from two types of medical images: computer tomography (CT) and magnetic resonance images (MRI). RALMs represent one sort of discrete orthogonal moments. RALMs extract the features from images using orthogonal moments to retrieve images from a database. Our approach is extensively assessed with noise-free and noisy images from three different benchmark databases: Emphysema-CT, NEMA CT, and NEMA MRI. The first two databases are used for CT image retrieval, while the third is for MR image retrieval. The proposed approach was tested against the state-of-the art local feature descriptors: Local Binary Pattern (LBP), and local diagonal extrema pattern (LDEP). It was also evaluated against orthogonal Fourier-Mellin moments (OFMMs) as a global descriptor. The comparison shows a significant improvement in favor of the proposed approach in terms of three different performance metrics: ARP, ARR, and F_score. The proposed approach was also compared against the convolutional neural network (CNN) as a deep learning based method over the NEMA-MRI dataset. The RALMs based approach showed a significant improvement when compared against two state-of-the-art medical image retrieval approaches: Histogram of Compressed Scattering Coefficients (HCSCs) and a local bit-plane decoding-based AlexNet descriptor (LBpDAD), the study has done over the TCIA-CT dataset. The proposed approach was also tested with big well-known dataset from the international skin imaging collaboration (ISIC) 2018.

INDEX TERMS Image retrieval systems, Laguerre moments, medical imaging.

I. INTRODUCTION

Everywhere in the world hospitals and medical institutes create and store a large variety of datasets of biomedical images (BMI) during the routine clinical practices. These datasets contain the images produced by the diverse biomedical modalities, which include X-Ray, ultrasound (US), computed tomography (CT), and magnetic resonance imaging (MRI). Such imaging modalities allow physicians to make their diagnosis effectively. The mastery to retrieve the BMI correctly is crucial for the researchers in medical sciences where: it helps the physicians to make precise diagnosis [1], it provides real-time decision support [2] and it has its benefits when used as a part of a radiology teaching system [3]. Also it used as a tool for teaching and research in the medical institutes. For these reasons, studies have recently carried out to specify the importance of biomedical image retrieval (BMIR) as a core area of research.

Images can be recognized and retrieved via content-based image retrieval (CBIR) systems. Rao *et al.* [4], introduced CBIR system using Exact Legendre Moments (ELM) [5] for gray scale images. Rao and Rao [6], introduced a CBIR system to retrieve natural and texture images. Mudhafar *et al.* [7], proposed an effective image retrieval method based on a

The associate editor coordinating the review of this manuscript and approving it for publication was Zhenhua Guo.

new support vector machine NSVM and convolution neural network CNN. BMIR systems represent one type of image retrieval systems based totally on the extraction of appropriate features (i.e. shape, color, texture, etc). There are two main types of features: local and global. Global features describe the entire image, while local features describe the part or some parts of the image. Global features usually used in object detection, classification, and image retrieval, whereas the local descriptors used for object identification or recognition. It observed that the texture feature is the most common amongst many BMIR systems [8]–[12]. However, because of the importance of medical images, only texture feature is not sufficient to describe the image, hence the aggregate of many descriptors such as texture, shape, edges, etc., is required for constructing an efficient BMIR system.

The medical images are available in a different format. But we restricted our study with only two types of biomedical images: CT and MRI. The earliest studies on CT and MRI introduced by Manjunath *et al.* [13]. Felipe *et al.* [14], suggested the co-occurrence matrix (CM) technique for CT and MRI images. Unary *et al.* [15], introduced a robust and fast retrieval system for MRI of brain images. Ojala *et al.* [16], suggested an efficient texture feature descriptor called local binary pattern (LBP). Based on LBP, the feature vector formed through the intensity of each pixel. LBP, joint LBP, and image intensity histograms are used by Sørensen *et al.* [17], to make quantitative analysis to CT images of pulmonary emphysema. Peng *et al.* [18], introduced a feature extractor technique primarily based on the structure and the local brightness to analyze the CT images of the chest. Hosny *et al.* [19], presented an accurate method based on orthogonal moments for the reconstruction of noisy medical images. Quddus and Basir [20], introduced an approach based on noisy and multimodal observations to retrieve the 2-D MRI images. Murala and Wu presented essential contributions concerning the retrieval of CT and MRI images [21]–[23]. Moreover, Murala *et al.* [21] introduced a local ternary co-occurrence pattern (LTCoP). Later on Murala and Wu [22] suggested a strategy to retrieve BMI known as local mesh pattern (LMeP). The method presented in [22] developed to construct an algorithm called LMePVEP [23].

Local diagonal extrema pattern (LDEP) is a novel strategy introduced by Dubey *et al.* [24] to retrieve CT images. The main idea of LDEP is that the local extremes for local diagonals computed through first-order derivatives for local diagonals. The relationship between the central pixel and its neighbors computed via the comparison amongst the central pixel's intensity value and the local extrema of its neighbors. Later on Dubey *et al.* [25] suggested another method called LWP. According to LWP, the local wavelet decomposition for the local neighborhood of any pixel computed. Then the values obtained are compared with the transformed values of the central pixel. LWP calculated for all pixels of the image. Finally, the histogram computed as a feature vector. Depending on a novel method called local bit plane dissimilarity pattern (LBDISP) Dubey *et al.* [26] introduced the BMIR system for CT images. LBDISP proposed to handle the problem of both less discriminative and high discriminative. Based on LBDISP, Dubey *et al.* [27] suggested a new technique named as, local bit-plane decoded pattern (LBDP). The main reason that makes LDEP and its variants superior over other methods such as LBP, LTCoP, and LMeP is the high performance with shallow dimension in the feature vector.

Deep *et al.* [28] suggested a new technique named directional local ternary quantized extrema pattern (DLTerQEP) for BMIR. The proposed strategy exceeds the LBP, where it considers the pixels around the central pixel through four directions: 0°, 45°, 90°, and 135°. In contrast, the LBP considers only the local region around the central pixel. Deep *et al.* [29] introduced a novel local feature vector for MRI, and CT BMI named local mesh ternary pattern (LMeTP), which also based on ternary patterns. Recently, Deep *et al.* [30] introduced a new descriptor called local quantized extrema quinary pattern (LQEQryP) for BMI indexing and retrieval pattern. Verma and Raman [31] introduced a novel texture descriptor for image retrieval, and it named as, local tri-directional pattern (LTDP). Most of the previous local patterns consider only the center pixel for information extraction; according to LTDP, all pixels in the neighborhood found where they compared with the nearest pixels and center pixel for pattern information. Another feature descriptor called local neighborhood difference pattern (LNDP) is introduced by Verma and Raman [32], based on the differences in the intensity of the pixel. Pang *et al.* [33] introduced BMIR and indexing system based on deep preference learning.

Rehman S. U *et al.* introduced several studies for seizure effective image features using Convolutional neural network (CNN), hence using it in machine learning applications [34]–[38]. Lan *et al.* [39] introduced medical image retrieval system for CT images. They used scattering transform and particular variation of deep convolutional networks to derive texture characteristics of medical CT images then a novel feature, named histogram of compressed scattering coefficients (HCSCs), using the scattering representations of CT images is introduced. Dubey *et al.* [40] suggested biomedical image retrieval system called a local bit-plane decoding-based AlexNet descriptor (LBpDAD). It combines the advantages of local bit-plane decoded features and the convolutional neural network-based features such as AlexNet.

Several pre-mentioned methods have an essential role in BMI retrieval and many other pattern matching applications, but still, the main problem is that all of them are local descriptors. Medical datasets classified into different classes based on two different criteria. These criteria include both the images that represent the whole body parts and the images that describe the type of tissues of the same part or organ. Subsequently, the descriptors used with BMI must have the ability to differentiate between the entire BM images of various body parts and also between the local changes in the shape or the texture of the same organ. Thus both local and global descriptors are required for efficient retrieval of BM images. Global descriptors are also required to differentiate

between the images of various body parts. In contrast, local descriptors can distinguish between the different kinds tissues of the same organ (like, tumorous or non-tumorous) or the same structure (like the shape of ventricular in brain MRI). The reason behind the failure of the pre-mentioned techniques to be highly efficient in retrieving BM images not only their local nature but also their low performance against noisy datasets; since BM images sometimes may be noisy in life.

Kumar *et al.* [41] proposed an efficient approach based on Zernike moments as a global descriptor to retrieve CT and MRI images. Ashutosh *et al.* [42] introduced a new global descriptor based on orthogonal Fourier-Mellin moments (OFMMs) for efficient indexing and retrieval of BM images: CT and MRI.

Laguerre moments represent one type of discrete orthogonal moments [43], [44]. The experimental results obtained by Qjidaa *et al.* [43] specified the effectiveness of Laguerre moments as feature descriptors. Bojun *et al.* [44] suggested a kind of discrete orthogonal moments called RALMs for invariant pattern recognition and image reconstruction. The numerical results obtained in [44] proved that RALMs perform better than orthogonal Fourier-Mellin Moments (OFFMs) in image reconstruction and rotation invariant for both noisy and free noisy images. So, RALMs will be more appropriate for BMIR applications. So, in this study, we present a retrieval system based on RALMs for biomedical uses.

The current study encompasses some contributions that can be summarized as follows:

- A novel method was introduced for BMIR based on RALMs. It is useful and efficient, as it can capture multi-pronged edge information, texture, shapes and structural from BMI.
- Elaborated experiments were performed to specify the performance and ability of the RALMs to retrieve the BM images against other state-of-the-art approaches. The results show the superiority of the proposed method over the compared methods on three medical datasets: Emphysema-CT, NEMA CT, and NEMA MRI.
- Other experiments were performed to specify the out-perform of the proposed approach with noisy images.

The remainder of this study comes in four sections as follows: Section 2 discusses, in brief, the compared techniques. The proposed RALMs-based retrieval approach presented in Section 3. Our results figured and discussed in Section 4. Finally, section 5 offers a conclusion.

II. FEATURE EXTRACTION TECHNIQUES

In the following subsections, the study briefly explains the local and global descriptors included in the comparison: LBP, LDEP, and OFMMs.

A. LBP TECHNIQUE

Ojala *et al.* [16] proposed an LBP operator. This operator was used by Sørensen *et al.* [17] to make quantitative analysis for

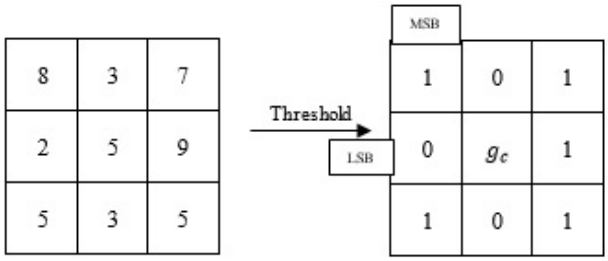

FIGURE 1. An example of LBP operator with a 3 × 3 window.

the CT of pulmonary emphysema. LBP distinguishes each pixel in the image with a decimal value called LBPs code. This decimal value has been resulted from the subtraction of the central pixel's value from its surrounding pixel values. If the resulting value is negative, it is encoded to 0; otherwise, it is encoded to 1. As shown in Fig.1, the binary code 10111010 occurred as a result of concatenating all the binary values in a clockwise direction starting from the value at the northwest corner. The decimal value equivalent to the binary code 10111010 would be 186, this value is called the LBPs code for the given 3 × 3 window.

Consider a pixel at (x_c, y_c), then LBP at (x_c, y_c) is obtained in decimal form as:

$$LBP_{N,R}(x_c, y_c) = \sum_{s=0}^{N-1} Th(g_s - g_c)\, 2^s \tag{1}$$

where, g_c and g_s represent gray values of that pixel at the center and the other pixels around it, R is the radius of the circle neighborhood pixels, and N is the number of pixels in the neighborhood of the central pixel.

The threshold function $Th(x)$ is defined as:

$$Th(x) = \begin{cases} 1 & if\ x \geq 0; \\ 0 & otherwise; \end{cases} \tag{2}$$

The most popular form of LBP is $LBP_{8,1}$. It used in a variety of applications in imaging sciences and also used for retrieval of MRI and CT images. The main advantage of LBP is the simplest form of its formula and also the simplicity of its implementation.

Ojala *et al.* [16] proposed the LBP for the texture analysis in the first place. Then, its uses has expanded to comprise image analysis [45], [46], retrieval of images and videos [47], [48], environment modeling [49], [50], visual inspection [51], [52], motion analysis [53], [54], biomedical and atmospheric image analysis [55], [56], remote sensing [57], and so on. The main problem of LBP is that its feature vector has a high dimension; this creates a problem in its computational complexity. For example, in the case of $LBP_{8,1}$, The feature vector contains 256 features from a single image. These features represent the binary codes acquired from the eight surrounding neighbors. To overcome that drawback, LBP extended to ULBP. U is known as the measure of uniformity, and it refers to the number of the bits transitioned between

0 and 1. LBP is called ULBP if U ≤ 2. For example, patterns like 11111111 (0 transitions), 10001111 (2 transitions), and 00110000 (2 transitions) are ULBP, while 00110110 (4 transitions), and 10101000 (5 transitions) are LBP.

B. LDEP TECHNIQUE

Dubey *et al.* [24], presented a new technique called LDEP. They used it as a retrieval system for CT images. As in [24], LDEP demonstrated high performance over many other approaches such as LTP, LTCoP, LMeP, etc. Therefore, LDEP is used to compare RALMs-based approaches. LDEP approach uses the first derivative of the local diagonal to find the values and indexes of the local diagonal extrema to take advantage of the linkage among any pixel at the center and its neighbors at the local diagonal. What makes LDEP more efficient is that it considers only the diagonal neighbors. So, the dimension of the feature vector shrinks, and the retrieval task consequently increases in speed.

LDEP for any central pixel (x, y) calculated as follows:

At first, the difference between the value of the pixel at the center (x, y) and its local diagonal extrema computed as illustrated below

$$\Delta_{max}^{x,y} = I_{\varphi_{max}}^{x,y} - I^{x,y}, \tag{3}$$
$$\Delta_{min}^{x,y} = I_{\varphi_{min}}^{x,y} - I^{x,y}, \tag{4}$$

both $I_{\varphi_{min}}^{x,y}$ and $I_{\varphi_{max}}^{x,y}$ refer to the intensity values of the local diagonal extremes of the pixel (x, y).

The relationship among the central pixel and its local diagonal extrema is defined as

$$R = \begin{cases} 0, & if \ \left(sign\left(\Delta_{max}^{x,y}\right) = 0 \ and \ sign\left(\Delta_{min}^{x,y}\right) = 0\right) \\ 1, & if \ \left(sign\left(\Delta_{max}^{x,y}\right) = 1 \ and \ sign\left(\Delta_{min}^{x,y}\right) = 1\right), \\ 2, & otherwise \end{cases} \tag{5}$$

such that,

$$sign\left(\lambda\right) = \begin{cases} 1, & if \ \lambda \geq 0 \\ 0, & if \ \lambda < 0. \end{cases} \tag{6}$$

Finally, the components of the LDEP vector of a pixel (x, y) computed as

$$LDEP_J^{x,y} = \begin{cases} 1, & if \ J = (\varphi_{max} + 8R) \ or \ J = (\varphi_{min} + 4 + 8R), \\ 0, & otherwise \end{cases} \tag{7}$$

where, $LDEP_J^{x,y}$ is the component number J.

Hence, the LDEP feature vector for any pixel (x, y) is given by:

$$LDEP^{x,y} = \left(LDEP_1^{x,y}, LDEP_2^{x,y}, \ldots, LDEP_{dim}^{x,y}\right), \tag{8}$$

where *dim* is the length of the vector.

C. OFMMS TECHNIQUE

OFMMs were firstly introduced by Sheng and Shen [58] for invariant pattern recognition. For the function $f\ (r, \varphi)$, OFMMs of order n and repetition l is defined as

$$\varphi_{nl} = \frac{n+1}{\pi} \int_0^{2\pi} \int_0^1 Q_n(r) e^{-il\varphi} f\left(r, \varphi\right) r dr d_\varphi,$$
$$n = 0, 1, 2, \ldots, l = 0, \pm 1, \pm 2, \ldots, \tag{9}$$

where $Q_n(r)$ is the radial function that is defined as

$$Q_n\left(r\right) = \sum_{s=0}^{n} (-1)^{n+s} \frac{(n+s+1)!}{(n-s)!s!(s+1)!} r^s. \tag{10}$$

The radial function $Q_n\left(r\right)$ is orthogonal over the range $0 \leq r \leq 1$

$$\int_0^1 Q_n\left(r\right) Q_m\left(r\right) r dr = \frac{1}{2\left(n+1\right)} \delta_{mn}, \tag{11}$$

δ_{mn} is the Kronecker delta, and $r = 1$ is the maximum size of any encountered object in a particular application. Hence the basis functions $Q_n(r)e^{-il\varphi}$ are orthogonal over the interior of the unit circle.

For digital images, it required to use the modified form of (9) which introduced by Sheng *et al.* [58],

$$\varphi_{nl} = \frac{4\left(n+1\right)}{\pi N^2} \sum_{i=0}^{N-1} \sum_{k=0}^{N-1} Q_n\left(r_{i,k}\right) e^{-il\varphi_{ik}} f\left(x_i, y_k\right), \tag{12}$$

where the coordinates (x_i, y_k) are given by

$$x_i = \frac{2i+1-N}{N}, \quad y_k = \frac{2k+1-N}{N},$$
$$i, k = 0, 1, 2, \ldots, N-1$$

III. PROPOSED RADIAL ASSOCIATED LAGUERRE MOMENTS (RALMS)- BASED IMAGE RETRIEVAL SYSTEM

In this section, we propose the RALMs as a global descriptor to retrieve the biomedical images. The ALMs [43] is one kind of discrete orthogonal moments. ALMs defined in the existence of the associated Laguerre polynomials (ALPs) [60]–[62] (basis functions), which are orthogonal over the whole right-half plane.

ALMs of the image $I\left(x, y\right)$ with an order of $m + n$ and a size of NxN are defined as follows:

$$\tilde{M}_{mn}^{\alpha}\left(x\right) = \sum_{x=0}^{N-1} \sum_{y=0}^{N-1} \tilde{L}_m^{\alpha}\left(x\right) \tilde{L}_n^{\alpha}\left(y\right) I\left(x, y\right),$$
$$m, n = 0, 1, 2, \ldots, N-1 \tag{13}$$

where, $\left\{L_m^{\alpha}\right\}$, for $\alpha > -1$ are the ALPs that are orthogonal to the weight function $w\left(x\right) = x^{\alpha} e^{-x}$ on the interval $0 \leq x \leq +\infty$, that is

$$\int_0^{\infty} e^{-x} x^{\alpha} L_n^{\alpha}\left(x\right) L_m^{\alpha}\left(x\right) dx = \frac{\Gamma(n+\alpha+1)}{n!} \delta_{nm} m, n \geq 0 \tag{14}$$

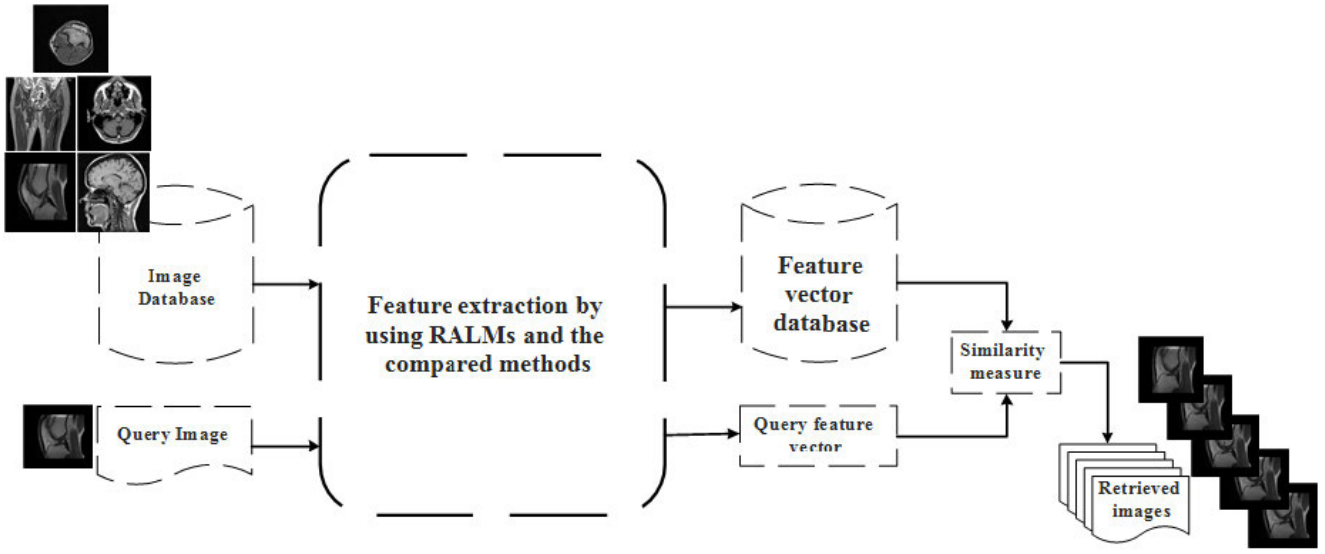

FIGURE 2. Flowchart of the proposed retrieval system RALMs.

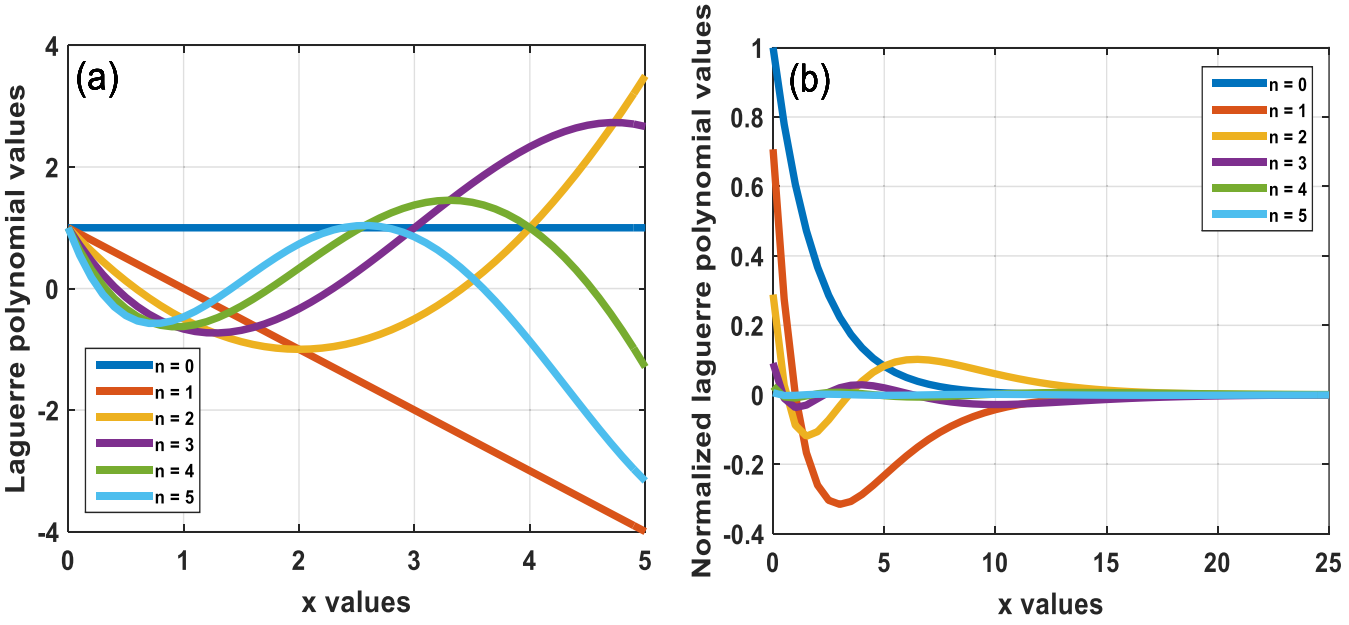

FIGURE 3. Plot (a) Laguerre polynomial values and (b) Normalized laguerre polynomial values at $\alpha = 0$.

where, δ_{nm} is a Kronecker delta, $\delta_{nm} = 1$ if $m = n$ and $\delta_{nm} = 0$ otherwise.

The ALPs defined as:

$$L_n^{\alpha}(x) = \sum_{k=0}^{n} \frac{(n+\alpha)!}{(n-k)!\,(k+\alpha)!k!} x^k \tag{15}$$

but due to the high increase of the polynomial values with increasing of the order, we restrict our study with the normalized orthogonal ALPs $\tilde{L}_n^{\alpha}(x)$, that is defined as:

$$\tilde{L}_n^{\alpha}(x) = \sqrt{\frac{e^{-x}x^{\alpha}n!}{(n+k)!}} L_n^{\alpha}(x) \tag{16}$$

As shown in Fig. (3) and Fig. (4) it is noted that the values of the normalized polynomials $\tilde{L}_n^{\alpha}(x)$ are bounded on a finite interval, a thing that doesn't occur with non-normalized polynomials $L_n^{\alpha}(x)$.

As shown in (13) ALMs are defined over the Cartesian coordinates so that it is not suitable for identifying the rotational invariance, so that we have the motive to define the RALMs of order p and repetition l as

$$\tilde{RM}_{pl}^{\alpha} = \frac{1}{2\pi} \sum_{r=0}^{m-1} \sum_{\theta=0}^{2\pi} \tilde{L}_p^{\alpha}(r)\, e^{-jl\theta} I(r,\theta), \tag{17}$$

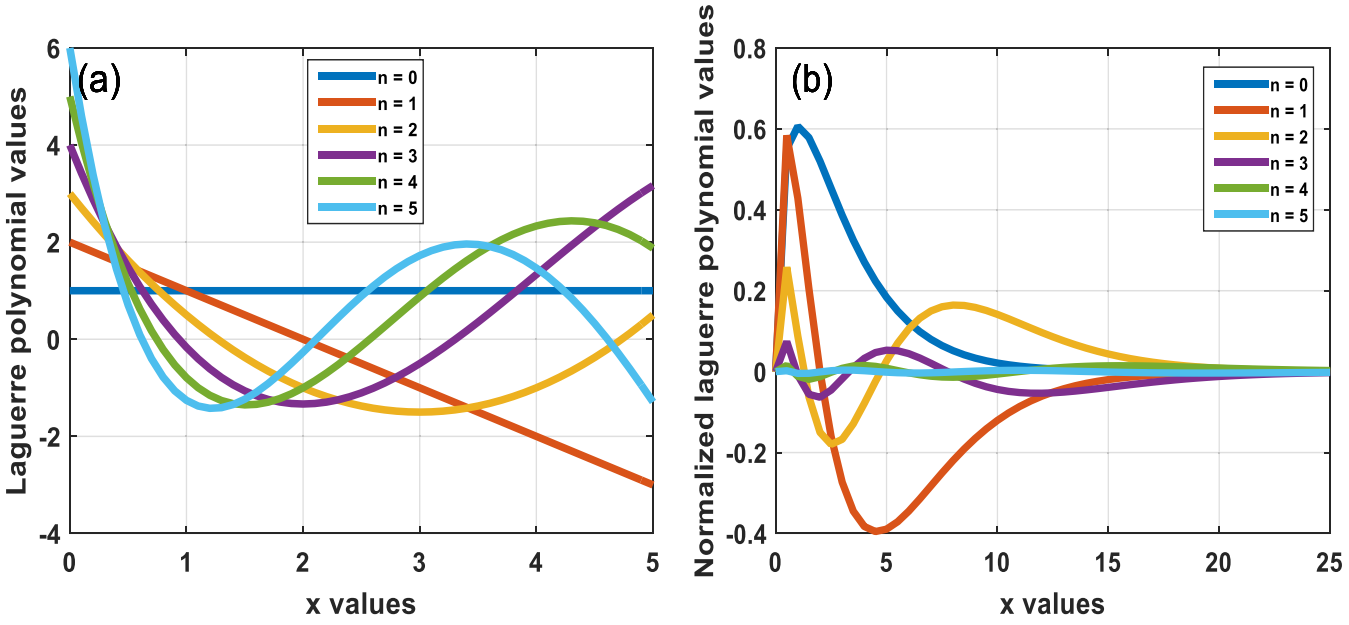

FIGURE 4. Plot (a) Laguerre polynomial values and (b) Normalized laguerre polynomial values at $\alpha = 1$.

where, $I(r, \theta)$, refers to the image intensity function in polar coordinates. The image has a size of $N \times N$ pixels, and m denotes $N/2$. Since θ is a real quantity measured in radians, one can rewrite (17) as follow:

$$\tilde{RM}_{pl}^{\alpha} = \frac{1}{n} \sum_{r=0}^{m-1} \sum_{\theta=0}^{n-1} \tilde{L}_{p}^{\alpha}(r)\, e^{-jl\theta} I(r, \theta), \tag{18}$$

where n is at 360.

Radial representation aims to deduce the rotation invariants easily as follow:

consider the image $I(r, \theta)$, which become $I(r, \theta + \emptyset)$ after rotation by angle $\emptyset$. In this case, RALMs represent as

$$\widehat{RM}_{pl}^{\alpha} = \frac{1}{2\pi} \int_{r=0}^{1} \int_{\theta=0}^{2\pi} \tilde{L}_{p}^{\alpha}(r)\, I(r, \theta + \varphi)\, e^{-jl(\theta+\varphi)} r d\theta dr, \tag{19}$$

$$\widehat{RM}_{pl}^{\alpha} = \frac{e^{-jl\varphi}}{2\pi} \int_{r=0}^{1} \int_{\theta=0}^{2\pi} \tilde{L}_{p}^{\alpha}(r) I(r, \theta)\, e^{-jl\theta} r d\theta dr, \tag{20}$$

$$\widehat{RM}_{pl}^{\alpha} = e^{-jl\varphi} \left[\frac{1}{2\pi} \int_{r=0}^{1} \int_{\theta=0}^{2\pi} \tilde{L}_{p}^{\alpha}(r) I(r, \theta)\, e^{-jl\theta} r d\theta dr \right], \tag{21}$$

from (17), one can deduce the following

$$\widehat{RM}_{pl}^{\alpha} = e^{-jl\varphi} \tilde{RM}_{pl}^{\alpha}, \tag{22}$$

$$\left\| \widehat{RM}_{pl}^{\alpha} \right\| = \left\| e^{-jl\varphi} \tilde{RM}_{pl}^{\alpha} \right\| = \left\| e^{-jl\varphi} \right\| . \left\| \tilde{RM}_{pl}^{\alpha} \right\|, \tag{23}$$

$$\left\| e^{-jl\varphi} \right\| = \sqrt{(\cos(-l\varphi))^2 + (\sin(-l\varphi))^2} = 1, \tag{24}$$

then

$$\left\| \hat{R}_{pl}^{\alpha} \right\| = \left\| \tilde{R}_{pl}^{\alpha} \right\|, \tag{25}$$

From (25) It evident that RALMs are with rotational invariance.

The value of the parameter α has an essential role in pattern recognition. It controls the shifting to the image region of interest. The authors in [40] proved that the most accurate recognition occurs at the values of α from 6 to 10 in case of noisy and noisy free images, so that, in our study, we use the same values.

The superiority of the RALMs in many image recognition applications in noise-free and noisy cases is due to the following worthwhile properties:

1. RALMs represent orthogonal moments, where it's basis functions are orthogonal. Hence each RALM coefficient can capture distinctive and unique parts of the image, also no redundancy in the information.
2. The magnitudes of RALMs coefficients are approximately the same in both cases of noisy free and noisy images. Hence RALMs would be robust against noisy images.
3. RALMs are robust against image rotation and scaling, where the magnitudes of RALMs coefficients are approximately the same for the image before and after either rotation or scaling.
4. The basis functions of RALMs can capture different unique types of information from the image based on the different values of order. These unique features are average intensity value, variance, texture information, and edge information in a different orientation. Together, these

features provide the best representation of an image, where they represent a multidimensional view of an image.

5. For the compared method except for OFMMs, the feature values of an image can change when rotating or scaling the image. They can also change in case of noisy images. This change in the values of the features is due to the representation of those values, where it represents the differences between the center pixel and its neighbors in the spatial domain. These inter-pixel differences tend to change with any changes in the image, such as rotation, scaling, and noisy cases. However, in the case of RALMs, it's values are still the same before and after any change in the image because of its orthogonality property. Therefore, RALMs are more suitable for real-life applications such as BMIR

IV. EXPERIMENTAL RESULTS AND DISCUSSIONS

In the following subsections, the study exposes the datasets that used to test our strategy. It also discusses the experimental results in detail through some evaluation measures.

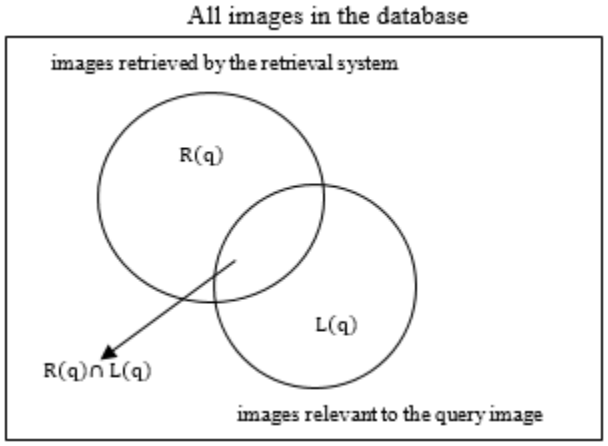

FIGURE 5. Venn diagram to specify the meaning of precision and recall.

FIGURE 6. Example images from the Emphysema-CT database, one image from each group.

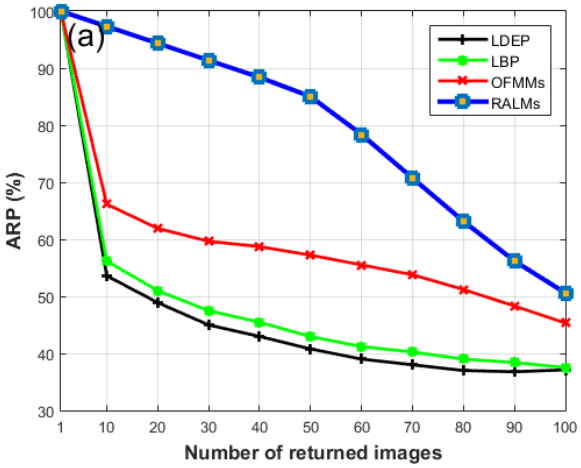

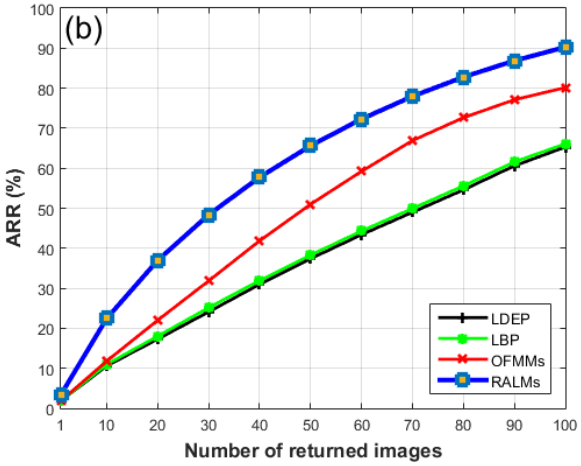

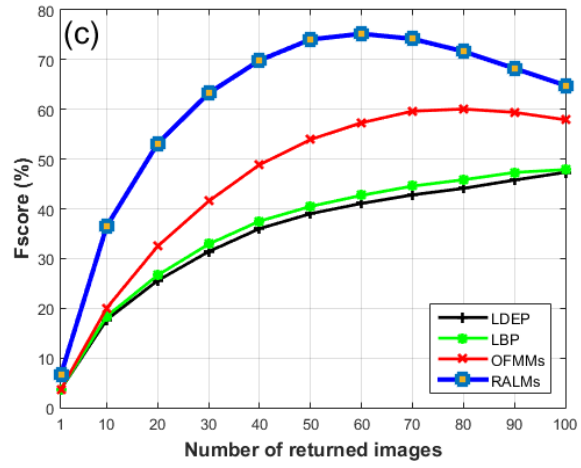

FIGURE 7. Comparison of the RALMs technique with the other compared approaches by passing various query images (1-100) in case of (a) ARP (b) ARR (c) F_score on Emphysema-CT dataset.

A. DATASETS

The evaluation of our system done through three benchmark datasets.

Emphysema-CT dataset: The first dataset [63] comprises 168 tissue images of the same body part for 39 various cases. Images in Emphysema-CT come in three classes based on the texture of lung tissues: Centrilobular Emphysema (CLE) that contain 50 images, Normal tissue (NT) that

includes 59 images and Paraceptal Emphysema (PSE) that contain 59 images.

The NEMA-CT dataset: The second dataset [64] consists of different categories of CT images for different body parts that created to assist in the research and diagnosis purpose. In our study, we considered the following cases of NEMA-CT database: CT0001, CT003, CT0021, CT0030, CT0031, Ct0053, CT0054, CT0057, CT0060, and CT0083. We collected 608 CT images have the dimension 512 × 512. These images represent different body parts. Images are grouped into 10 classes having 54, 60, 66, 50, 15, 60, 52, 104, 75 and 69 images.

The NEMA-MRI dataset: The third dataset [65] contains different categories of MRI images for different body parts. The study considered the following datasets cases: BRAINSAG, LOCKNEE, MOVEKNEE, MOVEKNIN, MOVEKNINT, VOLBRAIN, VHMFLGSM, and KNEE3D. In this study, we collected 371 MRI images that have the dimension 256 × 256. These images are categorized into five categories having 60, 63, 72, 76, and 100 images.

As we mentioned that the BMI in the first database (Emphysema-CT) are of the same organ, while the second and the third (NEMA-CT and NEMA-MRI) comprise BMI for various organs. For better results, any retrieval system to give better results with such datasets, must have the ability to distinguish among the BM images that seem to be the same but are different locally as in the Emphysema-CT database. Also the retrieval system must have the ability to differentiate between the BM images which are globally different as in NEMA-CT and NEMA-MRI databases.

B. EVALUATION MEASURES

To specify the performance of our system, three experiments were carried out and showed in-detail through the following subsections. A comparison between the performance of the RALMs approach and other recently released approaches: LBP, LDEP, OFMMs, HCSCs and LBpDAD is performed. Further experiments were carried out under noisy conditions to specify the high efficiency of our approach as a retrieval system when compared with the other methods. In our study, we have used the same evaluation criteria used in [24]. To estimate the likeness between the feature vectors of two images, we use the following distance similarity measure

$$D_1(Q, DB) = \sum_{i=0}^{dim} \left| \frac{f_{DB_{ji}} - f_{Q_i}}{1 + f_{DB_{ji}} - f_{Q_i}} \right|, \tag{26}$$

where *dim* represents the length of the feature vectors; $f_{DB_{ji}}$ denotes ith feature for jth image and f_{Q_i} is the ith feature of the query image. Fig. 2 represents the framework of the proposed system.

The current study compared the performance of the present approach with the existing methods through two evaluation measures. These measures used by Murla and Jonathan [21], [24] are called average retrieval precision (ARP), and average retrieval rate (ARR). ARP was also used by Girgis and Reda [66]. We used another performance measure called *F_score*.

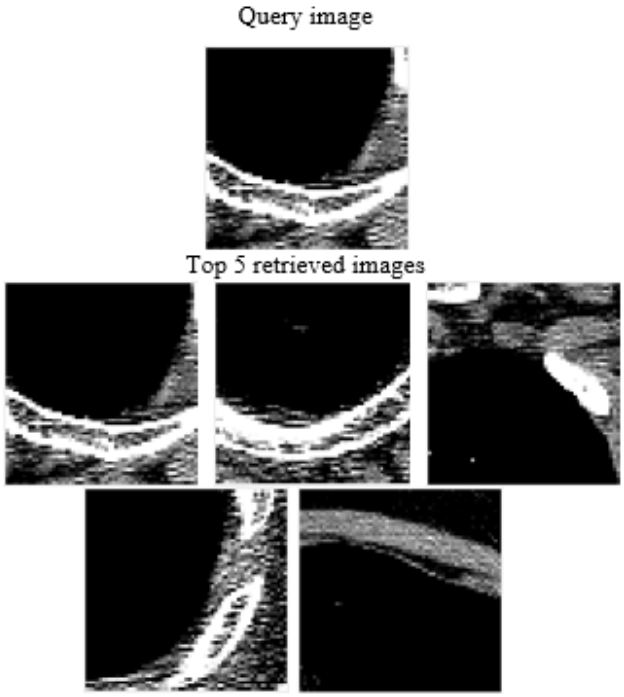

FIGURE 8. The retrieved images using RALMs for a query from the Emphysema-CT database.

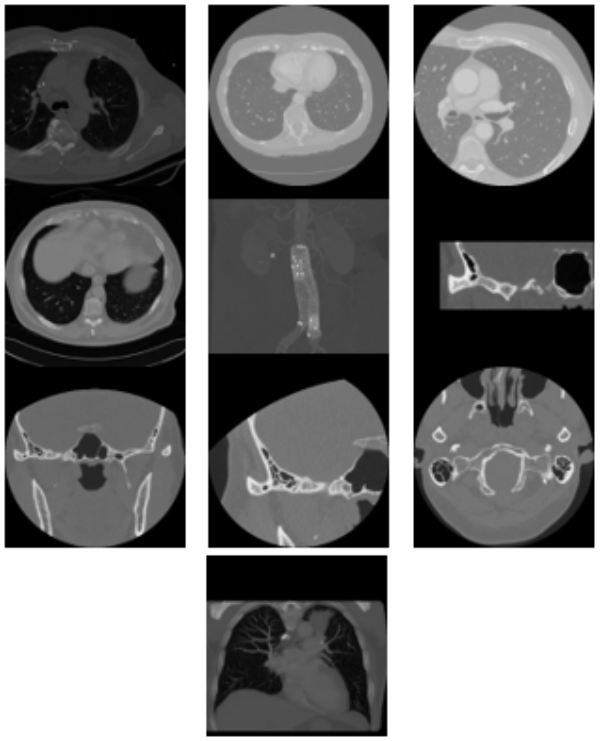

FIGURE 9. Example images from the NEMA-CT database, one image from each group.

As shown in Fig. 5. q is a query image, R(q) represents the set of all images that are retrieved by our system, and L(q) represents the set of all images that are relevant to the query image. Precision and recall defined as follow: -

$$precision{:}P\,(q) = \frac{|\mathrm{R(q)} \cap \mathrm{L(q)}|}{|\mathrm{R(q)}|} \tag{27}$$

$$recall{:}R\,(q) = \frac{|\mathrm{R(q)} \cap \mathrm{L(q)}|}{|\mathrm{L(q)}|} \tag{28}$$

where the $|\bullet|$ operator represents the cardinality of a set (i.e., the number of objects in the collection). Hence, ARP and ARR can be defined as follow:

$$ARP\,(\%) = \frac{100}{|DB|}\sum_{i=1}^{|DB|} P\,(I_i) \tag{29}$$

$$ARR\,(\%) = \frac{100}{|DB|}\sum_{i=1}^{|DB|} R\,(I_i) \tag{30}$$

$$F\_score\,(\%) = \frac{2(ARP)(\mathrm{ARR})}{ARP + ARR} \tag{31}$$

where $|DB|$ represent the count of all images in the dataset. In our experiment, we consider every image in the dataset as a query image, while the rest images in the DB represent target images for the query.

C. EMPIRICAL FINDINGS OVER EMPHYSEMA-CT DATASET

Emphysema-CT database [63] exists mainly to help physicians diagnosing chronic obstructive pulmonary disease (COPD). The main characteristic of Emphysema is its ability to damage the lung tissues. Appropriate classification of healthy lung tissues and emphysematous is essential for accurate diagnosis of the disease. Fig. 6 depicts one image from each class of the Emphysema-CT Database. Fig. 7 shows the retrieval performance in terms of *ARP*, *ARR*, and *F_score* for the proposed RALMs technique against the compared methods at different values for the number of returned images.

TABLE 1. Improvement percentage in retrieval rates of RALMs when compared with the other methods on the Emphysema-CT dataset.

Performance metrics	*RALMs*	*OFMMs*	*LBP*	*LDEP*
	A	*B*	*C*	*D*
ARP	50.58	45.32	37.53	37.12
ARR	90.28	80.15	66.10	65.29
F_score	64.83	57.90	47.87	47.33
Efficiency gain = RALMs – compared method				
	A-B	*A-C*	*A-D*	
ARP	5.26	13.05	13.46	
ARR	10.13	24.18	24.99	
F_score	6.93	16.96	17.5	
Average efficiency gain	7.44	18.06	18.65	

Table1 summarizes the results of the performance measures. From table 1, one can observe that the RALMs approach is superior over LBP, LDEP, and OFMMs techniques in terms of the performance metrics: *ARP*, *ARR*, and *F_score*. The improvement in the retrieval rate for the proposed approach when compared with that of the existing methods is showed through table 1. The average gain of the RALMs approach increased in comparison with OFMMs, LBP, and LDEP approaches by the percentages 7.44%, 18.06%, and 18.65%, respectively, in terms of all the performance metrics. Fig. 8 presents the query results of the RALMs approach over the Emphysema-CT dataset.

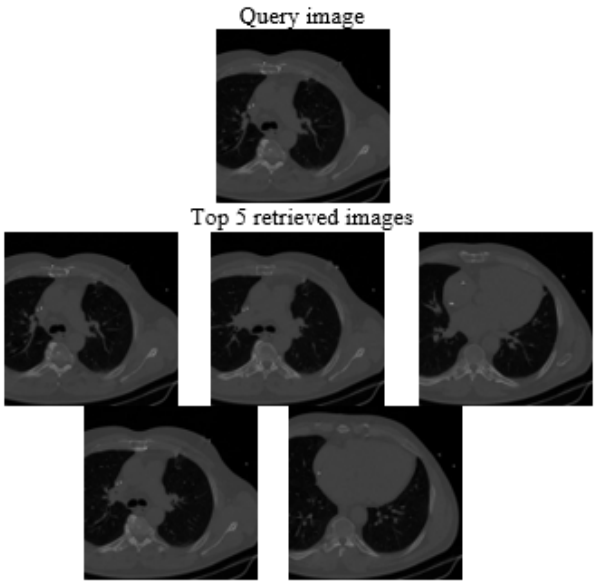

FIGURE 10. The retrieved images using RALMs for a query from NEMA-CT database.

TABLE 2. Improvement percentage in retrieval rates of RALMs when compared with the other methods on the NEMA-CT dataset.

Performance metrics	*RALMs*	*OFMMs*	*LBP*	*LDEP*
	A	*B*	*C*	*D*
ARP	76.14	67.71	62.28	64.73
ARR	99.21	97.45	94.22	95.26
F_score	86.16	79.90	74.99	83.05
Efficiency gain = RALMs – compared method				
	A-B	*A-C*	*A-D*	
ARP	8.43	13.86	11.41	
ARR	1.76	4.99	3.95	
F_score	6.26	11.17	3.11	
Average efficiency gain	5.48	10.006	6.15	

D. EMPIRICAL FINDINGS OVER NEMA-CT DATASET

The NEMA-CT (National Electrical Manufactures Association-Computed Tomography) [64] is an open-access information resource for medical researches. All image datasets are in DICOM format. Fig. 9 depicts sample images from each category of the dataset. Graphs in fig. 11 shows the excellence of the RALMs technique when it is compared with the other methods in terms of the performance measures *ARP*, *ARR*, and *F_score* at different values for the top matches. Table 2 summarizes the results obtained when comparing

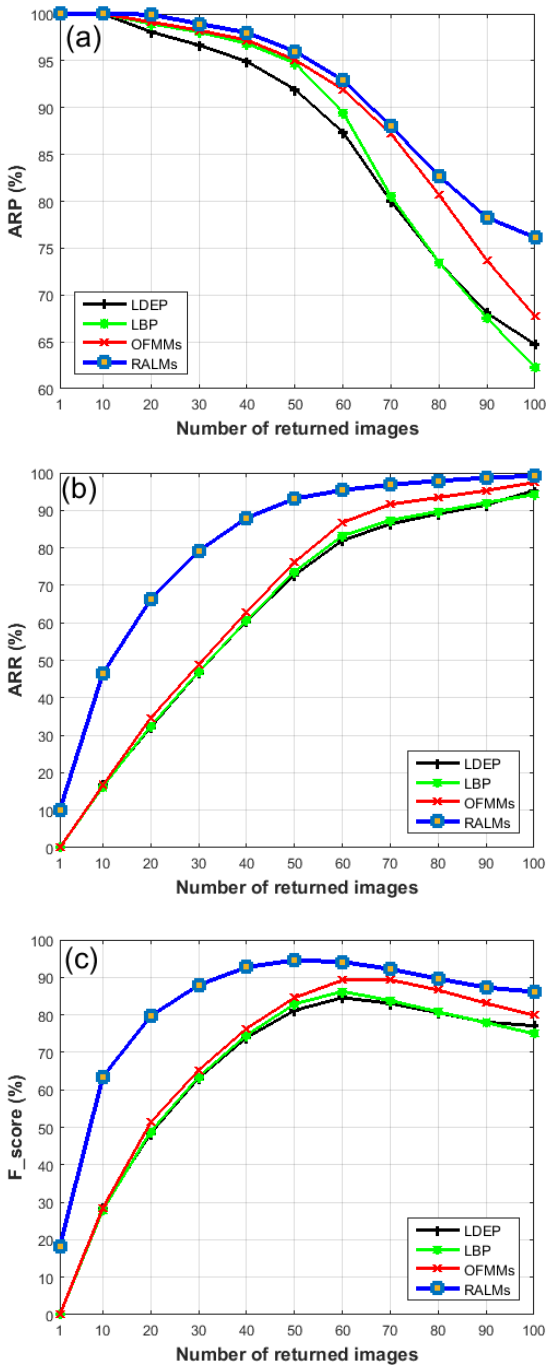

FIGURE 11. Comparison of the RALMs technique with the other compared approaches by passing various query images (1-100) in case of (a) ARP (b) ARR (c) F_score on NEMA-CT dataset.

the RALMs with the OFMMs, LBP, and LDEP approaches. From table 2, it is obvious that the average gain in retrieval rates of the three performance measures of RALMs comes in following percentages 5.48%, 10.006%, and 6.15% when compared with the approaches OFMMs, LBP and LDEP respectively. Fig. 10 depicts the query results of the RALMs-based approach over the NEMA-CT database. Results in table 1 and table 2 show the superiority of the retrieval process in case of NEMA-CT over that of Emphysema-CT. This

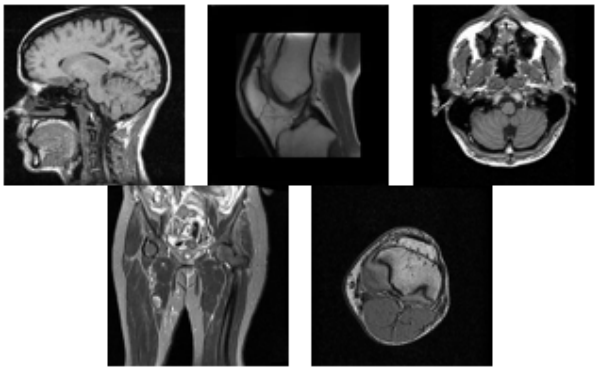

FIGURE 12. Example images from the NEMA-MRI database, one image from each group.

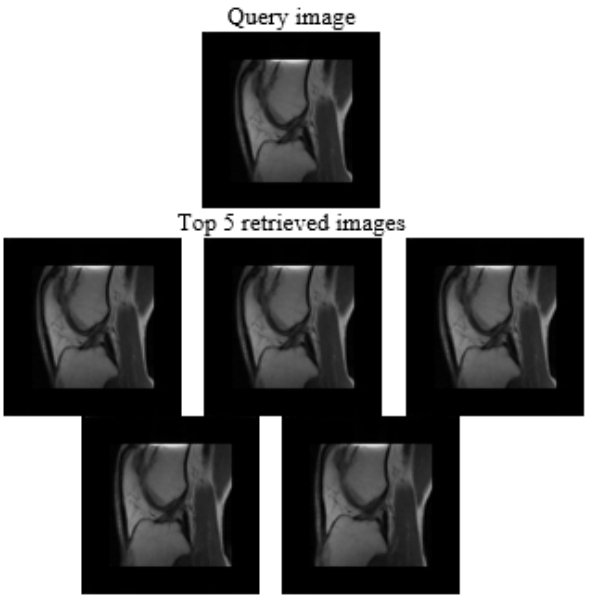

FIGURE 13. The retrieved images using RALMs for a query from the NEMA-MRI database.

superiority is due to that the three classes of Emphysema-CT contain images of different tissues of the same body part (i.e. lung) while each category in NEMA-CT includes images of various body parts. Hence, it is easy to distinguish between BM images of different organs if it is compared to images of the same lung tissue part.

E. EMPIRICAL FINDINGS OVER NEMA-MRI DATABASE

Magnetic resonance images (MRI) are helpful in diagnosis. They facilitate the distinction between the diseased and healthy tissues of the body. Fig. 12 depicts an example from different classes of the NEMA-MRI dataset [65]. Graphs in fig. 14 shows the superiority of the RALMs proposed approach over the compared methods in case of the performance metrics: *ARP*, *ARR*, and F_{score} at different values for the top matches images. Table 3 summarizes the results obtained when comparing the RALMs with the OFMMs, LBP, and LDEP approaches. From table 3, it is obvious

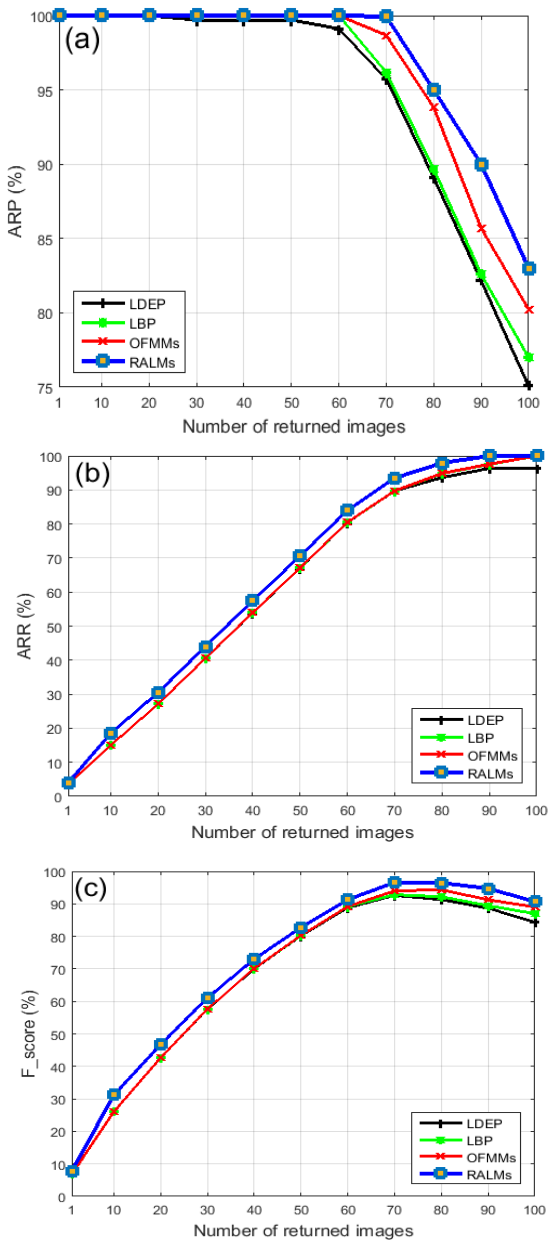

FIGURE 14. Comparison of the RALMs technique with the other compared approaches by passing various query images (1-100) in case of (a) ARP (b) ARR (c) F_score on the NEMA-MRI dataset.

that the average gain in retrieval rates of the three performance measures of RALMs comes in following percentages 1.48%, 3.24% and 6.09% when compared with the approaches OFMMs, LBP and LDEP respectively. The query results of the RALMs-based methods over the NEMA-MRI database are depicted in Fig. 13. Table 3 shows that the retrieval rate is higher in case of the NEMA-MRI dataset when compared to NEMA-CT. This occurs because NEMA-MRI, contains only five categories that are very different from each other as observed in Fig. 12. Hence the misclassification among these different categories would be very rare.

Furthermore, we investigated the efficiency of the proposed method (i.e. RALMs) against the convolutional neural network CNN as a deep learning based method over NEMA_MRI dataset. We used two sequence CNN layers with CNN architecture. The first uses 128 filters with kernel size of 3×3, while the second uses 64 filters with kernel size of 3×3. We used Max-Pooling technique in both two layers. Next a flatten layer followed by a fully-connected layer of 32 nodes. A dropout technique is applied with 0.4 value to decrease the overfitting, also all layers used RELU activation function. The comparison occurred with maximum number of returned images equal 60. Table 4, shows the obtained results over the three performance measures: ARP, ARR and F_score. The results specified the superiority of CNN in case of ARR and F_score but not in case of ARP. Despite of the superiority of CNN but still there are some challenges which push us to invest in such moments based approach (i.e. RALMs). The most important of these challenges are: lack of data, overfitting and imbalance datasets. All these challenges occur due to CNN requires huge number of data to train, the quality of data (i.e. noisy images or low quality images) and when number of images in some classes dominate over other classes respectively. All the pre mentioned problems push us to research in different approaches like the proposed approach (RALMs), which do not require any data to train and not affected by noise conditions as proved through subsection *F*.

TABLE 3. Improvement percentage in retrieval rates of RALMs when compared with the other methods on the NEMA-MRI database.

Performance metrics	*RALMs*	*OFMMs*	*LBP*	*LDEP*
	A	*B*	*C*	*D*
ARP	83	80.23	76.99	75.07
ARR	100	100	100	96.21
F_score	90.72	89.03	87	84.33
Efficiency gain = RALMs – compared method				
	A-B	*A-C*	*A-D*	
ARP	2.77	6.01	7.93	
ARR	0	0	3.79	
F_score	1.69	3.72	6.39	
Average efficiency gain	1.48	3.24	6.09	

TABLE 4. Comparison results between RALMs and CNN on the NEMA-MRI database. (all values are in percentage).

Methods	Evaluation Criteria		
	ARP	ARR	F_score
RALMs	100	84	91.30
CNN	97	97	97

F. EMPIRICAL FINDINGS OVER TCIA-CT DATABASE

The efficiency of the proposed approach was also compared against other two medical image retrieval approaches named HCSCs [39] and LBpDAD [40]. These two approaches were tested over a benchmark dataset called

The Cancer Image Archive (TCIA-CT) [67] as discussed in [39], [40]. TCIA contains a large number of cancer images. In our study we used the TCIA-CT dataset; it contains 604 Colo_prone 1.0 B30f CT images in DICOM format with series number 1.3.6.1.4.1.9328.50.4.2 of study instance UID 1.3.6.1.4.1.9328.50.4.1 for subject 1.3.6.1.4.1.9328.50.4.0001. TCIA-CT dataset is divided into 8 classes having 75, 50, 58, 140, 70, 92, 78 and 41 images. Fig. 15 depicts a sample image from each class. As reported in [39], [40], in the current study we used 10 images as a maximum number of returned images. The retrieval performance in terms of ARP, ARR and Fscore is shown in table 5 and the obtained results show a significant improvement in favor of the proposed approach. The average gain in retrieval rates of the three performance measures of RALMs comes in following percentages 0.9840% and 1.5207% when compared with the approaches LBpDAD and HCSCs respectively. Fig. 16 depicts the query results of the RALMs-based approach over the TCIA-CT dataset.

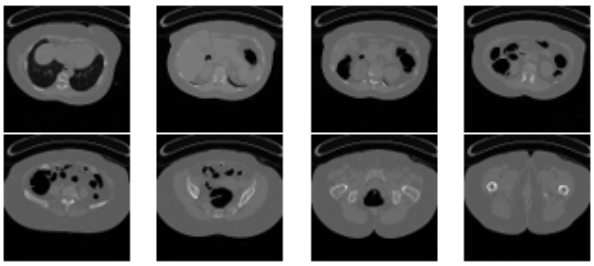

FIGURE 15. Sample images from each class of TCIA-CT dataset.

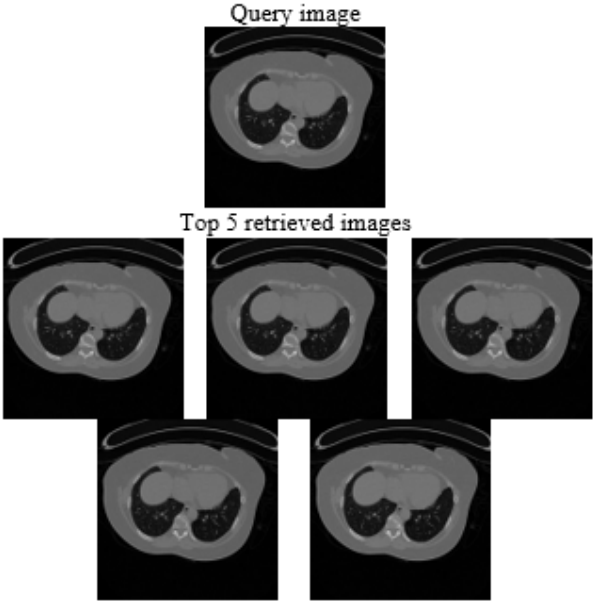

FIGURE 16. The retrieved images using RALMs for a query from TCIA-CT database.

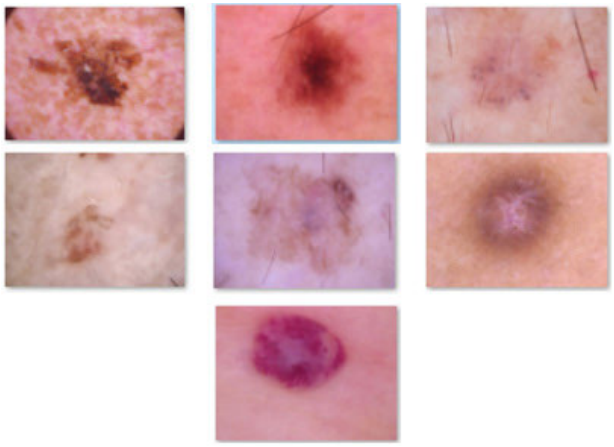

FIGURE 17. Sample images from each class of ISIC 2018 dataset.

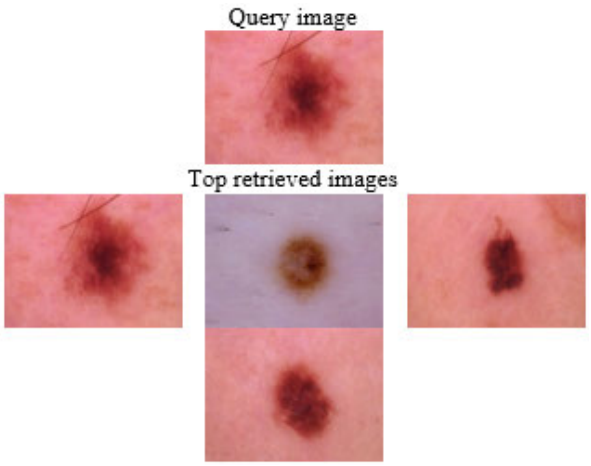

FIGURE 18. The retrieved images using RALMs for a query image from the ISIC 2018 dataset.

FIGURE 19. Example images from the Gaussian white noise Emphysema-CT database, one image from each group.

G. EMPIRICAL FINDINGS OVER ISIC 2018 DATABASE

The proposed approach was also tested over a big well-known database from the International Skin Imaging Collaboration (ISIC) 2018 [68]. This database contains 10,015 skin images, grouped into seven classes: MEL contains 1113, NV contains 6705 images, BCC contains 514 images, AKIEC contains 327 images, BKL contains 1099 images, DF contains 115 images, and VASC contains 142 images. Fig. 17 depicts one sample image from each class.

The retrieval performance in terms of ARP, ARR and Fscore with maximum number of 100 returned images is

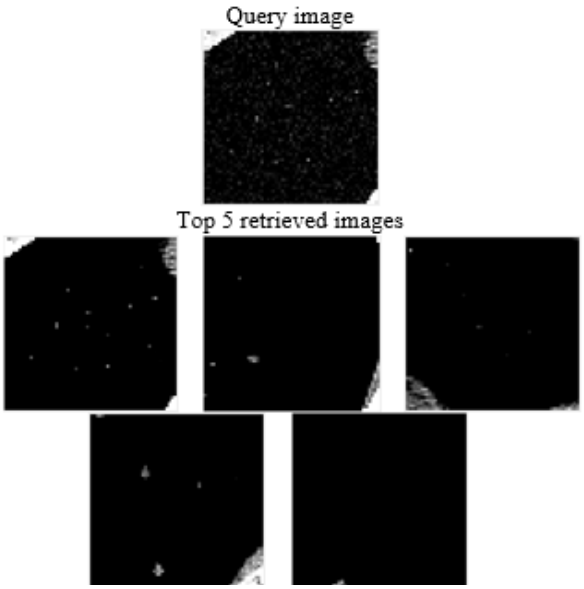

FIGURE 20. The retrieved images using RALMs for a query from a noisy Emphysema-CT database.

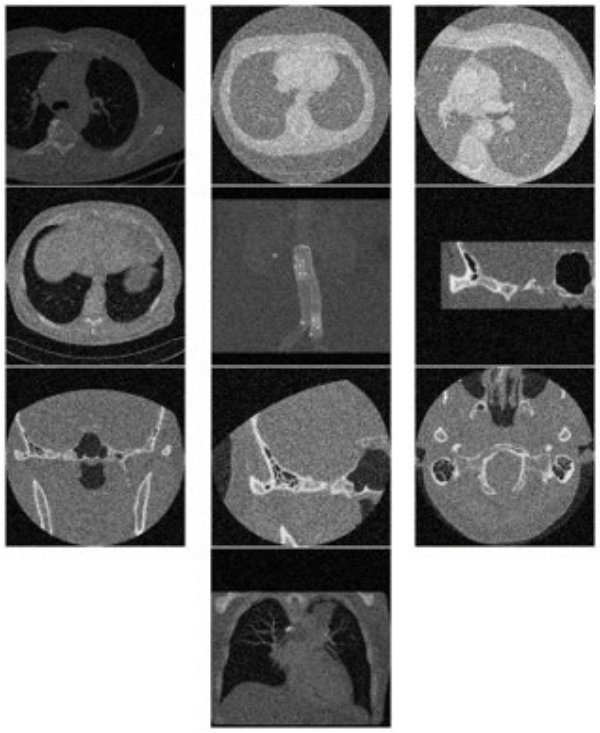

FIGURE 21. Example images from the Gaussian white noise NEMA-CT database, one image from each group.

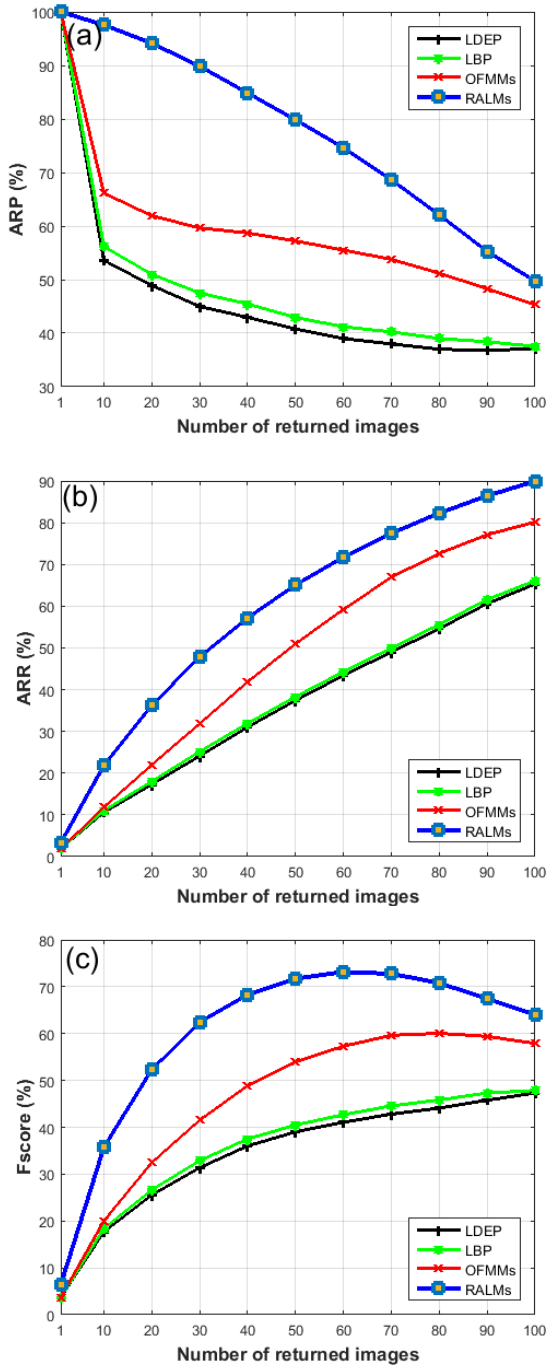

FIGURE 22. Comparison of the RALMs technique with the other compared approaches by passing various query images (1-100) in case of (a) ARP (b) ARR (c) F_score on Gaussian white noise Emphysema-CT database.

shown in table 6. According to the results obtained in table 6, the retrieval rate is low when compared to the results obtained by NEMA-CT and NEMA-MRI. Furthermore, this low rate is attributed to that the seven classes of ISIC 2018 contain different images for the same body part (i.e., skin), while each class in both NEMA-CT and NEMA-MRI contains images of various body parts. Hence, it is easy to distinguish between images of different organs if this is compared to images of the same part. Fig. 18 depicts the query results of the RALMs-based approach over the ISIC 2018 dataset. It is worthy noted that the query image and the retrieved images are of the same class (i.e., NV).

H. EMPIRICAL FINDINGS OVER NOISY DATABASES

The present study employs Gaussian white noise with zero means to test the efficiency of RALMs against the other

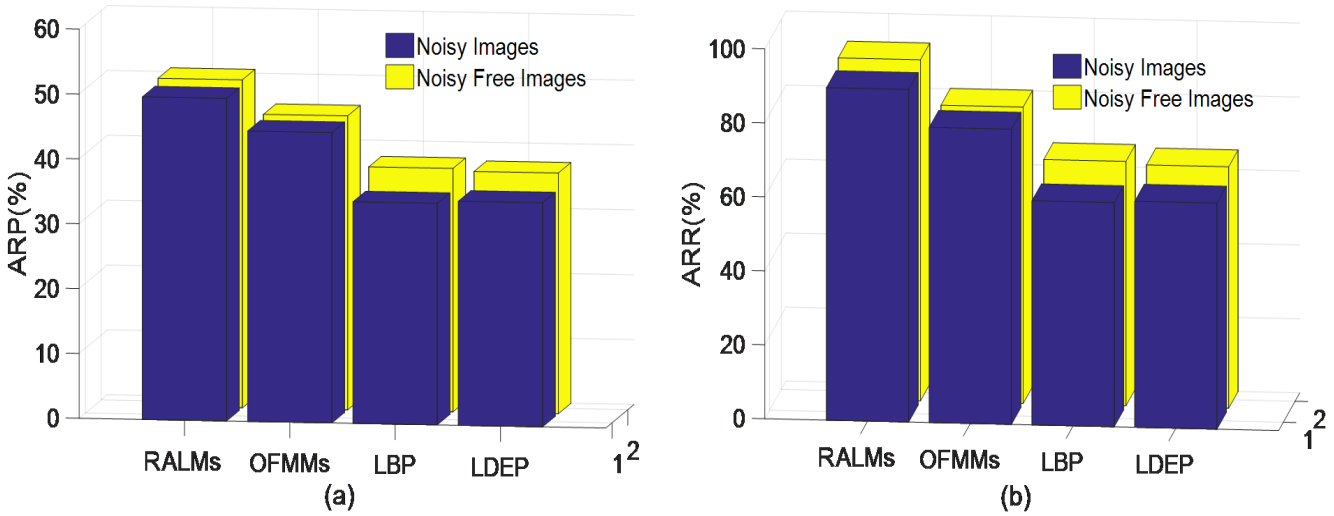

FIGURE 23. RALMs against the compared techniques in case of (a) ARP and (b) ARR in both cases of Gaussian white noise and noise-free Emphysema-CT.

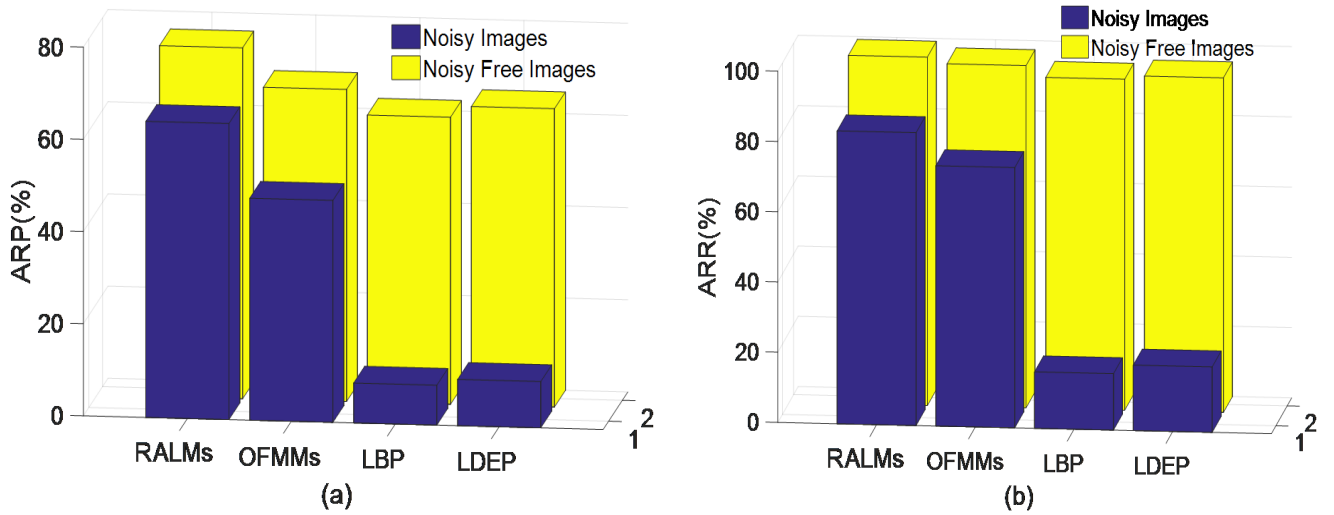

FIGURE 24. RALMs against the compared techniques in case of (a) ARP and (b) ARR in both cases of Gaussian white noise and noise-free NEMA-CT.

TABLE 5. Improvement percentage in retrieval rates of RALMs when compared with LBpDAD and HCSCs on the TCIA-CT database.

Performance metrics	*RALMs*	*LBpDAD*	*HCSCs*
	A	*B*	*C*
ARP	98.7500	96.32	95.12
ARR	14.8438	14.67	14.52
F_score	25.8082	25.46	25.20
Efficiency gain = RALMs – compared method			
	A-B	*A-C*	
ARP	2.4300	3.6300	
ARR	0.1738	0.3238	
F_score	0.3482	0.6082	
Average efficiency gain	0.9840	1.5207	

compared methods in case of noisy images. Figs. 19, 21, and 27 represent samples of noise images from the three datasets namely: Emphysema-CT, NEMA-CT, and NEMA-MRI databases respectively. Also. Figs. 22, 29, and 30 represent the retrieval performance of RALMs method against the compared approaches in case of ARP, ARR, and F_score at different values for the number of returned images. Tables 7, 9, and 12 show the retrieval rates for RALMs, that results are close to the results obtained in case of noise-free datasets for all performance metrics. Also from tables

TABLE 6. Results of RALMs on the ISIC 2018 dataset. (all values are in percentage).

Methods	Evaluation Criteria		
	ARP	ARR	F_score
RALMs	54	89	67

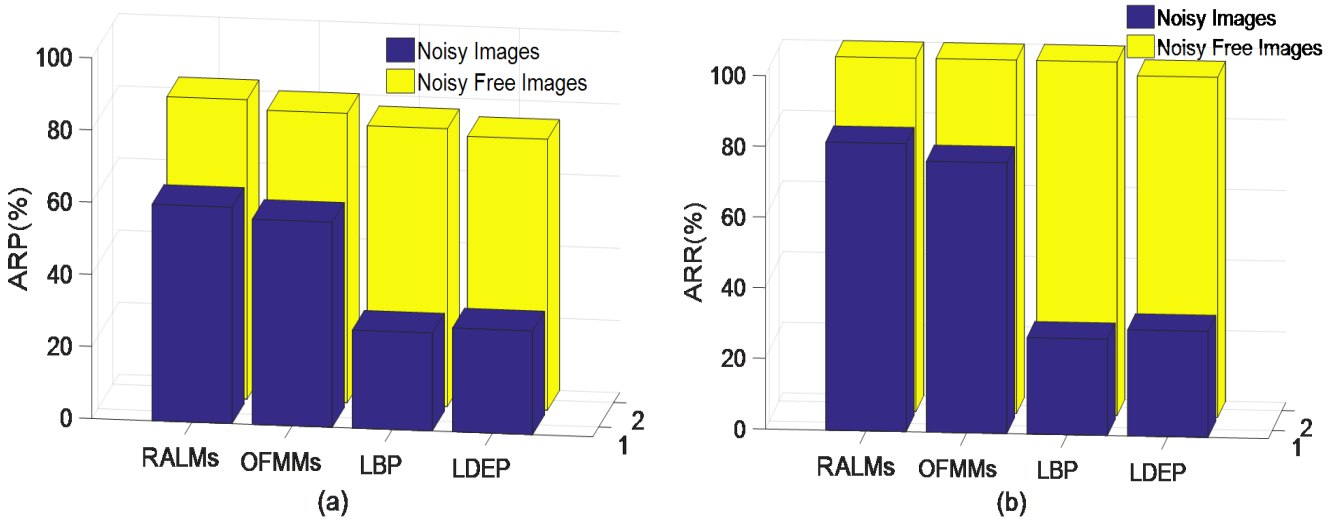

FIGURE 25. RALMs against the compared techniques in case of (a) ARP and (b) ARR in both cases of Gaussian white noise and noise-free NEMA-MRI.

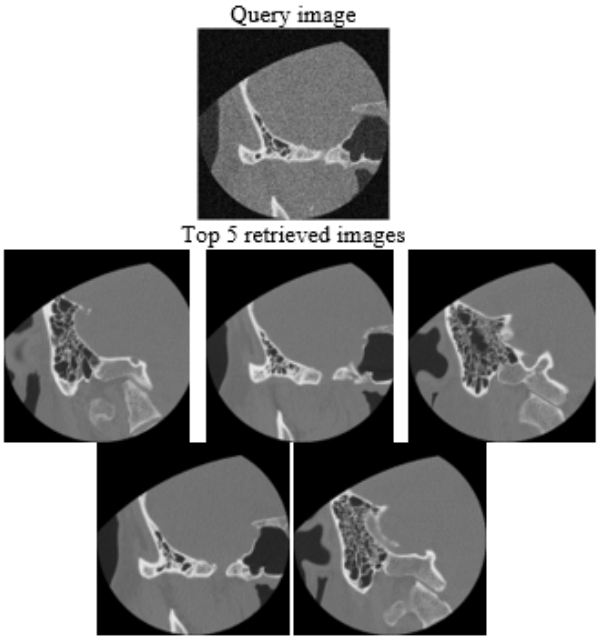

FIGURE 26. The retrieved images using RALMs for a query from a noisy NEMA-CT database.

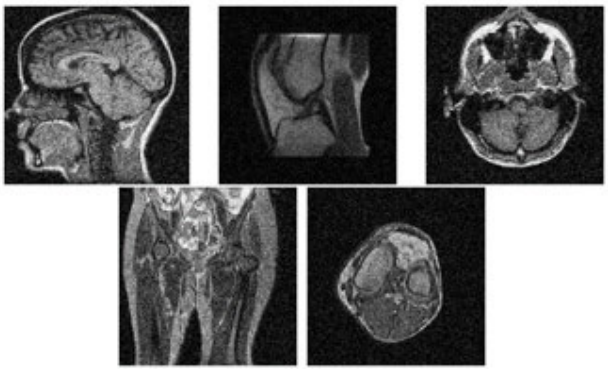

FIGURE 27. Example images from the Gaussian white noise NEMA- MRI database, one image from each group.

TABLE 7. Improvement percentage in retrieval rates of RALMs when compared with the other methods in case of Gaussian white noise with Emphysema-CT database.

Performance metrics	*RALMs*	*OFMMs*	*LBP*	*LDEP*
	A	*B*	*C*	*D*
ARP	49.73	44.77	34.16	34.55
ARR	89.93	79.84	60.63	61.15
F_score	64.04	57.37	43.69	44.15
Efficiency gain = RALMs – compared method				
	A-B	*A-C*	*A-D*	
ARP	4.96	15.57	15.18	
ARR	10.09	29.3	28.78	
F_score	6.67	20.35	19.89	
Average efficiency gain	7.24	21.74	21.28	

7, 9, and 12 we observed that the average efficiency gain in retrieval rates is in favor of RALMs at the expense of the compared methods for the three databases (Emphysema-CT, NEMA-CT, and NEMA-MRI) with the following percentages (7.24%, 21.74%, 21.28%), (13.17%, 61.14%, 66.14%) and (3.95%, 42.99%, 40.82%) respectively, overall the three performance measures. Figs. 23, 24, and 25 show a comparison between the proposed approach and the compared approaches in terms of ARP and ARR retrieval performance metrics, on noisy and noisy free cases of Emphysema-CT, NEMA-CT, and NEMA-MRI databases respectively.

We observed that the maximum drop for Emphysema-CT, NEMA-CT, and NEMA-MRI was in favor of LBP, followed by LDEP, then OFMMs in case of noisy datasets. For the noisy free datasets, the maximum drop was in favor of LDEP followed by LBP, then OFMMs in both of Emphysema-CT

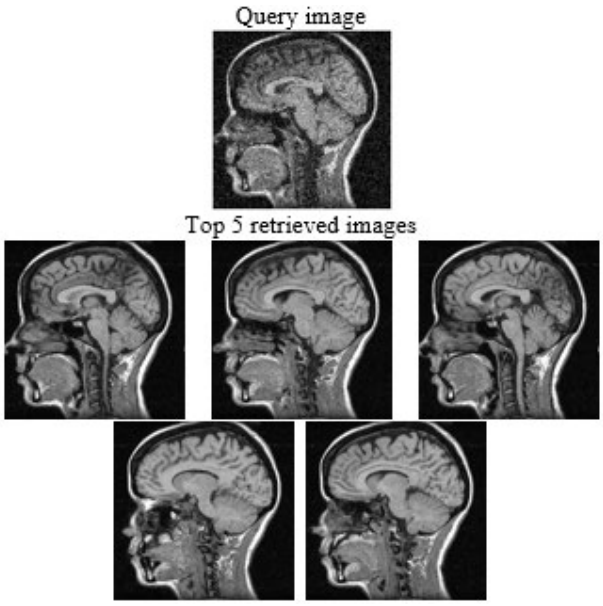

FIGURE 28. The retrieved images using RALMs for a query from Gaussian white noise NEMA-MRI database.

TABLE 8. Comparison results between the retrieval rates of RALMs in case of the two types of noise with Emphysema-CT database. (all values are in percentage).

Performance metrics	*RALMs with Gaussian noise*	*RALMs with Pepper & salt noise*
ARP	49.73	49.571
ARR	89.93	90.216
F_score	64.04	63.984

TABLE 9. Improvement percentage in retrieval rates of RALMs when compared with the other methods in case of Gaussian white noise with NEMA-CT database.

Performance metrics	*RALMs*	*OFMMs*	*LBP*	*LDEP*
	A	*B*	*C*	*D*
ARP	64.24	48.17	8.66	10.05
ARR	83.38	74.10	16.70	18.64
F_score	72.57	58.39	11.40	13.06
Efficiency gain = RALMs – compared method				
	A-B	*A-C*	*A-D*	
ARP	16.07	55.58	54.19	
ARR	9.28	66.68	64.74	
F_score	14.18	61.17	79.51	
Average efficiency gain	13.17	61.14	66.14	

TABLE 10. Comparison results between the retrieval rates of RALMs in case of the two types of noise with NEMA-CT database. (all values are in percentage).

Performance metrics	*RALMs with Gaussian noise*	*RALMs with Pepper & salt noise*
ARP	64.24	63.917
ARR	83.38	83.080
F_score	72.57	72.250

and NEMA-MRI, but in case of NEMA-CT the maximum reduction was in favor of LBP followed by LDEP then OFMMs. Figs. 20, 26, and 28 represent the query results of RALMs approach over noisy Emphysema-CT, noisy NEMA-CT, and noisy NEMA-MRI, respectively. From figs. 23, 24, and 25, we observed that there exists a drop in case of noisy images when compared to noisy free images on all three noisy test datasets in case of ARP and ARR performance measures. This drop is high in case of the compared methods but still relatively low with the proposed approach. All these indicators establish the truth of the robustness of the RALMs values against noisy conditions.

TABLE 11. Comparison results between the retrieval rates of RALMs in case of the two types of noise with NEMA-MRI database. (all values are in percentage).

Performance metrics	*RALMs with Gaussian noise*	*RALMs with Pepper & salt noise*
ARP	59.98	59.277
ARR	86.53	86.012
F_score	70.85	70.185

TABLE 12. Improvement percentage in retrieval rates of RALMs when compared with the other methods in case of Gaussian white noise with NEMA-MRI database.

Performance metrics	*RALMs*	*OFMMs*	*LBP*	*LDEP*
	A	*B*	*C*	*D*
ARP	59.98	56.85	27.15	28.76
ARR	81.53	76.64	27.28	30.02
F_score	69.11	65.28	27.21	29.38
Efficiency gain = RALMs – compared method				
	A-B	*A-C*	*A-D*	
ARP	3.13	32.83	31.22	
ARR	4.89	54.25	51.51	
F_score	3.83	41.9	39.73	
Average efficiency gain	3.95	42.99	40.82	

Furthermore, the study investigated the effectiveness of the proposed approach (RALMs) against another type of noise (i.e., Pepper & salt). Tables 8, 10 and 11 show the comparison between the retrieval performance of RALMs with Gaussian noise and Pepper & salt noise over noisy Emphysema-CT, noisy NEMA-CT, and noisy NEMA-MRI, respectively. The results obtained ensure the robustness of RALMs against the different types of noise. To avoid any redundancy, we plotted only the results concerning the Gaussian white noise.

V. CONCLUSION

In conclusion, this study presented a new retrieval system for biomedical images proposed using Radial Associated Laguerre Moments (RALMs) as a global descriptor. Thanks to the orthogonality of its basis functions (ALPs), which allow a multidimensional view of an image and invariant of the coefficients of RALMs. The performance of the proposed system assessed through several experiments that applied on three BM datasets: Emphysema-CT, NEMA-CT for computer tomography images, and NEMA-MRI for magnetic resonance images. The experiments performed with noise-free and noisy datasets. The numerical results after being investigated show a significant improvement in favor of the proposed approach against the compared techniques: OFMMs

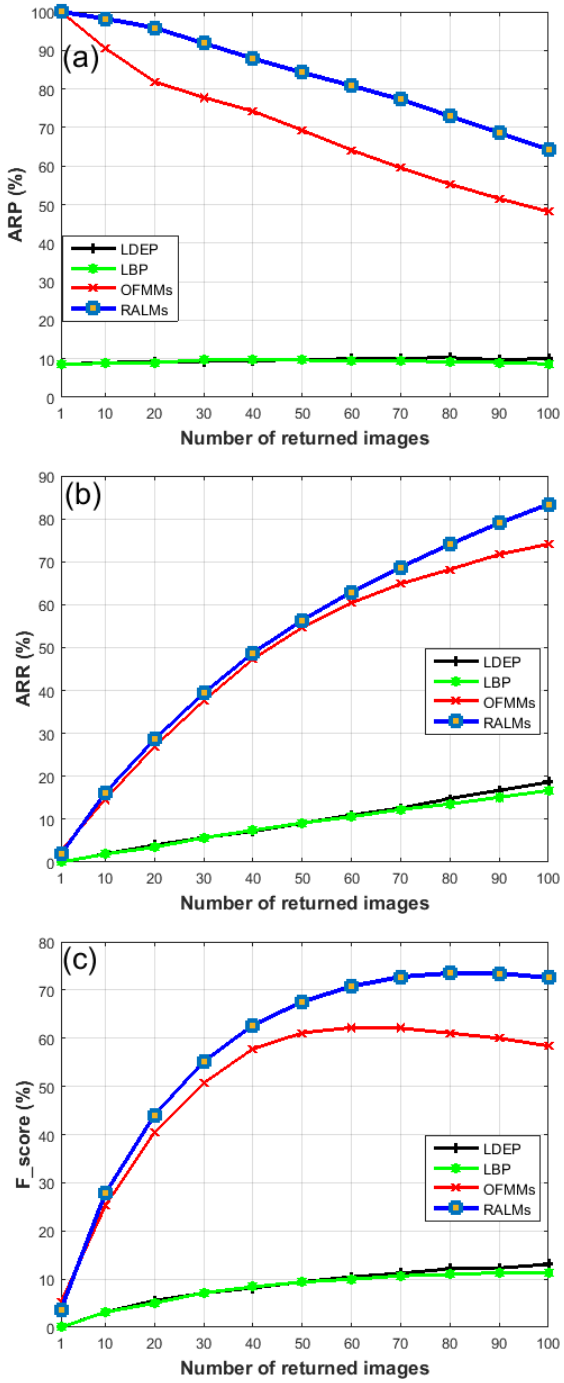

FIGURE 29. Comparison of the RALMs technique with the other compared approaches by passing various query images (1-100) in case of (a) ARP (b) ARR (c) F_score on Gaussian white noise NEMA-CT database.

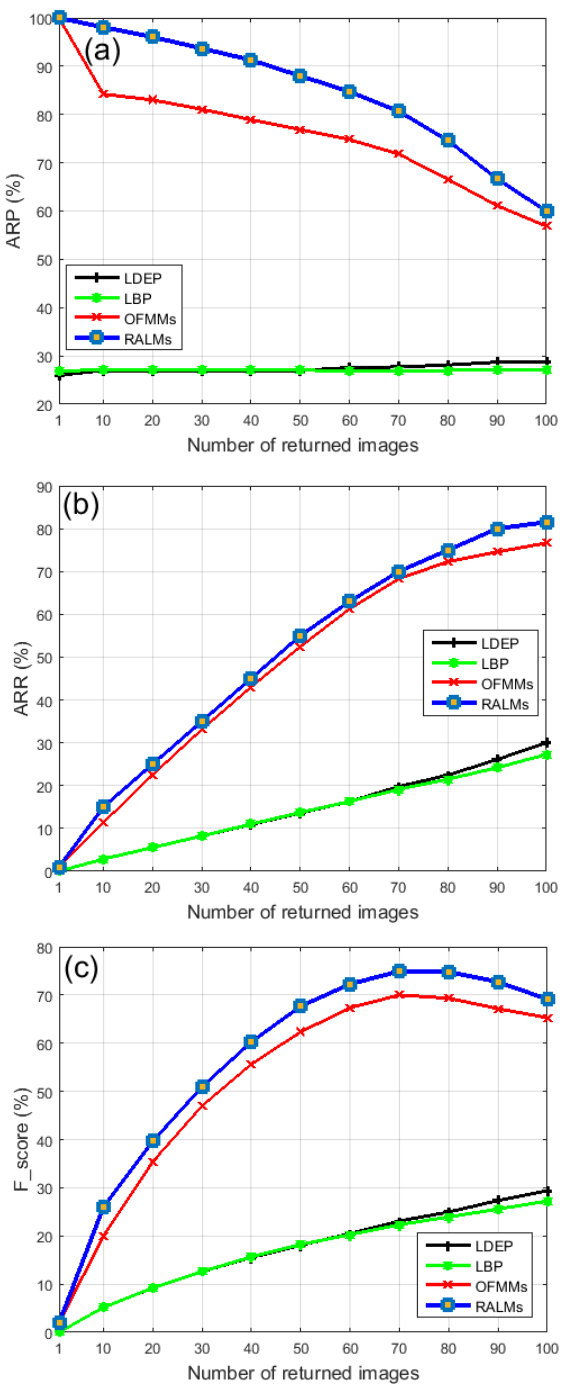

FIGURE 30. Comparison of the RALMs technique with the other compared approaches by passing various query images (1-100) in case of (a) ARP (b) ARR (c) F_score on Gaussian white noise NEMA-MRI database.

as a global descriptor, LBP, and LDEP as local descriptors in terms of the three performance measures ARP, ARR, and F_score. The RALMs based approach was also specified a significant improvement when compared with the HCSCs and the LBpDAD approaches over the TCIA-CT dataset. Good results obtained when tested the proposed approach over a big well-known dataset (i.e., ISIC 2018). Due to the leverage of the proposed approach in the case of gray medical images, it could upgrade through the quaternion concept that is applicable to color images.

REFERENCES

[1] A. M. Aisen, L. S. Broderick, H. Winer-Muram, C. E. Brodley, A. C. Kak, C. Pavlopoulou, J. Dy, C.-R. Shyu, and A. Marchiori, "Automated storage and retrieval of thin-section CT images to assist diagnosis: System description and preliminary assessment," *Radiology*, vol. 228, no. 1, pp. 70–265, 2003.

[2] S. A. Napel, C. F. Beaulieu, C. Rodriguez, J. Cui, J. Xu, A. Gupta, D. Korenblum, H. Greenspan, Y. Ma, and D. L. Rubin, "Automated retrieval of CT images of liver lesions on the basis of image similarity: Method and preliminary results," *Radiology*, vol. 256, no. 1, pp. 52–243, 2010.

[3] H. Müller, A. Rosset, A. Garcia, V. JP, and A. Geissbuhler, "Benefits of content-based visual data access in radiology," *Radiographics*, vol. 25, no. 3, pp. 58–849, 2005.

[4] C. S. Rao, S. S. Kumar, and B. C. Mohan, "Content based image retrieval using exact legendre moments and support vector machine," *Int. J. Multimedia Appl.*, vol. 2, no. 2, pp. 69–79, May 2010.

[5] K. M. Hosny, "Exact legendre moment computation for gray level images," *Pattern Recognit.*, vol. 40, no. 12, pp. 3597–3605, Dec. 2007.

[6] L. K. Rao and D. V. Rao, "Local quantized extrema patterns for content-based natural and texture image retrieval," *Hum.-Centric Comput. Inf. Sci.*, vol. 5, no. 1, pp. 26–50, Sep. 2015.

[7] M. J. J. Ghrabat, G. Ma, I. Y. Maolood, S. S. Alresheedi, and Z. A. Abduljabbar, "An effective image retrieval based on optimized genetic algorithm utilized a novel SVM-based convolutional neural network classifier," *Hum.-Centric Comput. Inf. Sci.*, vol. 9, no. 1, pp. 31–60, Aug. 2019.

[8] Y. Rui, T. S. Huang, and S.-F. Chang, "Image retrieval: Current techniques, promising directions, and open issues," *J. Vis. Commun. Image Represent.*, vol. 10, no. 1, pp. 39–62, Mar. 1999.

[9] A. W. M. Smeulders, M. Worring, S. Santini, A. Gupta, and R. Jain, "Content-based image retrieval at the end of the early years," *IEEE Trans. Pattern Anal. Mach. Intell.*, vol. 22, no. 12, pp. 1349–1380, Dec. 2000.

[10] M. Kokare, B. N. Chatterji, and P. K. Biswas, "A survey on current content based image retrieval methods," *IETE J. Res.*, vol. 48, nos. 3–4, pp. 261–271, Mar. 2015.

[11] Y. Liu, D. Zhang, G. Lu, and W.-Y. Ma, "A survey of content-based image retrieval with high-level semantics," *Pattern Recognit.*, vol. 40, no. 1, pp. 262–282, Jan. 2007.

[12] H. Muller, N. Michaux, D. Bandon, and A. Geisbuhler, "A review of content-based image retrieval systems in medical applications—Clinical benefits and future directions," *Int. J. Med. Inf.*, vol. 73, no. 1, pp. 1–23, Feb. 2004.

[13] K. N. Manjunath, A. Renuka, and U. C. Niranjan, "Linear models of cumulative distribution function for content-based medical image retrieval," *J. Med. Syst.*, vol. 31, no. 6, pp. 433–443, Oct. 2007.

[14] J. C. Felipe, A. J. M. Traina, and C. Traina, "Retrieval by content of medical images using texture for tissue identification," in *Proc. 16th IEEE Symp. Comput.-Based Med. Syst.*, New York, NY, USA, Jul. 2003, pp. 175–180.

[15] D. Unay, A. Ekin, and R. S. Jasinschi, "Local structure-based Region-of-Interest retrieval in brain MR images," *IEEE Trans. Inf. Technol. Biomed.*, vol. 14, no. 4, pp. 897–903, Jul. 2010.

[16] T. Ojala, M. Pietikäinen, and D. Harwood, "A comparative study of texture measures with classification based on featured distributions," *Pattern Recognit.*, vol. 29, no. 1, pp. 51–59, Jan. 1996.

[17] L. Srensen, S. B. Shaker, and M. de Bruijne, "Quantitative analysis of pulmonary emphysema using local binary patterns," *IEEE Trans. Med. Imag.*, vol. 29, no. 2, pp. 559–569, Feb. 2010.

[18] S.-H. Peng, D.-H. Kim, S.-L. Lee, and M.-K. Lim, "Texture feature extraction based on a uniformity estimation method for local brightness and structure in chest CT images," *Comput. Biol. Med.*, vol. 40, nos. 11–12, pp. 931–942, Nov. 2010.

[19] K. M. Hosny, G. A. Papakostas, and D. E. Koulouriotis, "Accurate reconstruction of noisy medical images using orthogonal moments," in *Proc. 18th Int. Conf. Digit. Signal Process. (DSP)*, Fira, Greece, Jul. 2013, pp. 1–6.

[20] A. Quddus and O. Basir, "Semantic image retrieval in magnetic resonance brain volumes," *IEEE Trans. Inf. Technol. Biomed.*, vol. 16, no. 3, pp. 348–355, May 2012.

[21] S. Murala and Q. M. Jonathan Wu, "Local ternary co-occurrence patterns: A new feature descriptor for MRI and CT image retrieval," *Neurocomputing*, vol. 119, no. 7, pp. 399–412, Nov. 2013.

[22] S. Murala and Q. M. J. Wu, "Local mesh patterns versus local binary patterns: Biomedical image indexing and retrieval," *IEEE J. Biomed. Health Informat.*, vol. 18, no. 3, pp. 929–938, May 2014.

[23] S. Murala and Q. M. Jonathan Wu, "MRI and CT image indexing and retrieval using local mesh peak valley edge patterns," *Signal Process., Image Commun.*, vol. 29, no. 3, pp. 400–409, Mar. 2014.

[24] S. R. Dubey, S. K. Singh, and R. K. Singh, "Local diagonal extrema pattern: A new and efficient feature descriptor for CT image retrieval," *IEEE Signal Process. Lett.*, vol. 22, no. 9, pp. 1215–1219, Sep. 2015.

[25] S. R. Dubey, S. K. Singh, and R. K. Singh, "Local wavelet pattern: A new feature descriptor for image retrieval in medical CT databases," *IEEE Trans. Image Process.*, vol. 24, no. 12, pp. 5892–5903, Dec. 2015.

[26] S. R. Dubey, S. K. Singh, and R. K. Singh, "Novel local bit-plane dissimilarity pattern for computed tomography image retrieval," *Electron. Lett.*, vol. 52, no. 15, pp. 1290–1292, Jul. 2016.

[27] S. R. Dubey, S. K. Singh, and R. K. Singh, "Local bit-plane decoded pattern: A novel feature descriptor for biomedical image retrieval," *IEEE J. Biomed. Health Informat.*, vol. 20, no. 4, pp. 1139–1147, Jul. 2016.

[28] G. Deep, L. Kaur, and S. Gupta, "Directional local ternary quantized extrema pattern: A new descriptor for biomedical image indexing and retrieval," *Eng. Sci. Technol., Int. J.*, vol. 19, no. 4, pp. 1895–1909, Dec. 2016.

[29] G. Deep, L. Kaur, and S. Gupta, "Local mesh ternary patterns: A new descriptor for MRI and CT biomedical image indexing and retrieval," *Comput. Methods Biomech. Biomed. Eng., Imag. Visualizat.*, vol. 6, no. 2, pp. 155–169, Mar. 2018.

[30] G. Deep, L. Kaur, and S. Gupta, "Local quantized extrema quinary pattern: A new descriptor for biomedical image indexing and retrieval," *Comput. Methods Biomech. Biomed. Eng. Imag. Vis*, vol. 6, no. 6, pp. 687–703, May 2017.

[31] M. Verma and B. Raman, "Local tri-directional patterns: A new texture feature descriptor for image retrieval," *Digit. Signal Process.*, vol. 51, pp. 62–72, Apr. 2016.

[32] M. Verma and B. Raman, "Local neighborhood difference pattern: A new feature descriptor for natural and texture image retrieval," *Multimedia Tools Appl*, vol. 55, no. 10, pp. 1–24, 2017.

[33] S. Pang, M. A. Orgun, and Z. Yu, "A novel biomedical image indexing and retrieval system via deep preference learning," *Comput. Methods Programs Biomed.*, vol. 158, pp. 53–69, May 2018.

[34] S. U. Rehman, S. Tu, Y. Huang, and Z. Yang, "Face recognition: A novel un-supervised convolutional neural network method," in *Proc. IEEE Int. Conf. Online Anal. Comput. Sci. (ICOACS)*, Chongqing, China, May 2016, pp. 139–144.

[35] S. ur Rehman, S. Tu, Y. Huang, and G. Liu, "CSFL: A novel unsupervised convolution neural network approach for visual pattern classification," *AI Commun.*, vol. 30, no. 5, pp. 311–324, Aug. 2017.

[36] S. Rehman, S. Tu, O. Rehman, Y. Huang, C. Magurawalage, and C.-C. Chang, "Optimization of CNN through novel training strategy for visual classification problems," *Entropy*, vol. 20, no. 4, pp. 290–300, Apr. 2018.

[37] S. U. Rehman, S. Tu, Y. Huang, and O. U. Rehman, "A benchmark dataset and learning high-level semantic embeddings of multimedia for cross-media retrieval," *IEEE Access*, vol. 6, pp. 67176–67188, 2018.

[38] S. U. Rehman, S. Tu, M. Waqas, Y. Huang, O. U. Rehman, B. Ahmad, and S. Ahmad, "Unsupervised pre-trained filter learning approach for efficient convolution neural network," *Neurocomputing*, vol. 365, pp. 171–190, Nov. 2019.

[39] R. Lan and Y. Zhou, "Medical image retrieval via histogram of compressed scattering coefficients," *IEEE J. Biomed. Health Informat.*, vol. 21, no. 5, pp. 1338–1346, Sep. 2017.

[40] S. R. Dubey, S. K. Roy, S. Chakraborty, S. Mukherjee, and B. B. Chaudhuri, "Local bit-plane decoded convolutional neural network features for biomedical image retrieval," *Neural Comput. Appl.*, vol. 32, no. 11, pp. 7539–7551, Jun. 2019.

[41] Y. Kumar, A. Aggarwal, S. Tiwari, and K. Singh, "An efficient and robust approach for biomedical image retrieval using Zernike moments," *Biomed. Signal Process. Control*, vol. 39, pp. 459–473, Jan. 2018.

[42] A. Aggarwal, S. Sharma, K. Singh, H. Singh, and S. Kumar, "A new approach for effective retrieval and indexing of medical images," *Biomed. Signal Process. Control*, vol. 50, pp. 10–34, Apr. 2019.

[43] H. Qjidaa, "Image reconstruction by Laguerre moments," presented at the 2nd Int. Symp. Commun., Control Signal Process. (ISCCSP), Marrakesh, Morocco, Mar. 15, 2006.

[44] B. Pan, Y. Li, and H. Zhu, "Image description using radial associated Laguerre moments," *J. ICT Res. Appl.*, vol. 9, no. 1, pp. 1–19, Jun. 2015.

[45] T. Ahonen, A. Hadid, and M. Pietikäinen, "Face recognition with local binary patterns," in *Proc. Eur. Conf. Comput. Vis.* Prague, Czech Republic: Springer, May 2004, pp. 469–481.

[46] A. Hadid, "The local binary pattern approach and its applications to face analysis," in *Proc. 1st Workshops Image Process. Theory, Tools Appl.*, Sousse, Tunisia, Nov. 2008, pp. 1–9.
[47] D. P. Huijsmans and N. Sebe, "Content-based indexing performance: Size normalized precision, recall, generality evaluation," in *Proc. Int. Conf. Image Process.*, Barcelona, Spain, Sep. 2003, pp. 3–733.
[48] D. Grangier and S. Bengio, "A discriminative kernel-based approach to rank images from text queries," *IEEE Trans. Pattern Anal. Mach. Intell.*, vol. 30, no. 8, pp. 1371–1384, Aug. 2008.
[49] W. Ali, F. Georgsson, and T. Hellstrom, "Visual tree detection for autonomous navigation in forest environment," in *Proc. IEEE Intell. Vehicles Symp.*, Eindhoven, The Netherlands, Jun. 2008, pp. 560–565.
[50] L. Nanni and A. Lumini, "Ensemble of multiple pedestrian representations," *IEEE Trans. Intell. Transp. Syst.*, vol. 9, no. 2, pp. 365–369, Jun. 2008.
[51] T. Mäenpää, J. Viertola, and M. Pietikäinen, "Optimising colour and texture features for real-time visual inspection," *Pattern Anal. Appl.*, vol. 6, no. 3, pp. 169–175, Dec. 2003.
[52] M. Turtinen, "Visual characterization of paper using isomap and local binary patterns," *IEICE Trans. Inf. Syst.*, vol. E89-D, no. 7, pp. 2076–2083, Jul. 2006.
[53] M. Heikkila and M. Pietikainen, "A texture-based method for modeling the background and detecting moving objects," *IEEE Trans. Pattern Anal. Mach. Intell.*, vol. 28, no. 4, pp. 657–662, Apr. 2006.
[54] P. A. Crook, V. Kellokumpu, G. Zhao, and M. Pietikainen, "Human activity recognition using a dynamic texture based method," in *Proc. Brit. Mach. Vis. Conf.*, M. Everingham C. Needham, Eds., 2008, p. 88.
[55] X. L. A. Oliver, J. Freixenet, and J. Martí, "False positive reduction in mammographic mass detection using local binary patterns," in *Proc. Med. Image Comput. Comput.-Assist. Intervent.*, Feb. 2007, pp. 286–293.
[56] S. Kluckner, G. Pacher, H. Grabner, H. Bischof, and J. Bauer, "A 3D teacher for car detection in aerial images," in *Proc. IEEE 11th Int. Conf. Comput. Vis.*, Rio de Janeiro, Brazil, Oct. 2007, pp. 1–8.
[57] A. S. A. Lucieer and P. Fisher, "Multivariate texture-based segmentation of remotely sensed imagery for extraction of objects and their uncertainty," *Int. J. Remote Sensing.*, vol. 26, no. 14, pp. 2917–2936, Feb. 2005.
[58] Y. L. Sheng and L. X. Shen, "Orthogonal Fourier-Mellin moments for invariant pattern recognition," *J. Opt. Soc. Amer. A, Opt. Image Sci.*, vol. 11, no. 6, pp. 1748–1757, Jun. 1994.
[59] C. Singh and R. Upneja, "Error analysis in the computation of orthogonal rotation invariant moments," *J. Math. Imag. Vis.*, vol. 49, no. 1, pp. 251–271, Aug. 2013.
[60] R. Askey and J. Wimp, "Associated Laguerre and Hermite polynomials," *Proc. Roy. Soc. Edinburgh Sect. A*, vol. 96, nos. 1–2, pp. 15–37, 1984.
[61] G. Sansone, *Orthogonal Functions*, Revised Ed. New York, NY, USA: Dover, Aug. 2004.
[62] R. A. El Attar, *Special Functions and Orthogonal Polynomials*. Raleigh, NC, USA: Lulu Press, 2006.
[63] *Emphy SEMA CT Database*. Accessed: Nov. 12, 2019. [Online]. Available: https://laugesoerensen.github.io/emphysema-database/
[64] *NEMA CT Image Database*. Accessed: Nov. 12, 2019. [Online]. Available: htttp://medical.nema.org/medical/Dicom/Multiframe/CT
[65] *NEMA MR Image Database*. Accessed: Nov. 12, 2019. [Online]. Available: htttp://medical.nema.org/medical/Dicom/Multiframe/MR
[66] M. R. Girgis and M. S. Reda, "A study of the effect of color quantization schemes for different color spaces on content-based image retrieval," *Int. J. Comput. Appl.*, vol. 96, no. 12, pp. 1–8, Jun. 2014.
[67] K. Clark, B. Vendt, K. Smith, J. Freymann, J. Kirby, P. Koppel, S. Moore, S. Phillips, D. Maffitt, M. Pringle, and L. Tarbox, "The cancer imaging archive (TCIA): Maintaining and operating a public information repository," *J. Digit. Imag.*, vol. 26, no. 6, pp. 1045–1057, 2013.
[68] (2018). *ISIC Archive*. Accessed: Aug. 22, 2020. [Online]. Available: https://challenge.isic-archive.com/data#2018

GABER HASSAN received the B.Sc. and M.Sc. degrees in math and computer sciences from the Faculty of Science, Zagazig University, Egypt, in 2007 and 2014, respectively. He is currently working as a Teaching Assistant with the Basic Sciences Department, Faculty of Engineering Sciences, Sinai University, Egypt. His research interests include image processing, computer vision, and bioinformatics.

KHALID M. HOSNY (Senior Member, IEEE) was born in Zagazig, Egypt, in 1966. He received the B.Sc., M.Sc., and Ph.D. degrees from Zagazig University, Egypt, in 1988, 1994, and 2000, respectively. From 1997 to 1999, he was a Visiting Scholar with the University of Michigan, Ann Arbor, MI, USA, and the University of Cincinnati, Cincinnati, OH, USA. He is currently a Professor of Information Technology with the Faculty of Computers and Informatics, Zagazig University. He has published three edited books and more than 70 papers in international journals. He is an editor and scientific reviewer for more than 35 international journals. His research interests include image processing, pattern recognition, multimedia, and computer vision. He is a Senior Member of the ACM.

RUSHDY MOHAMED FAROUK is currently working as an Assistant Professor of Computer Science with the Faculty of Science, Zagazig University, Egypt.

AHMED MANSOUR ALZOHAIRY received the Ph.D. degree in plant signal transduction from the Faculty of Agriculture, Zagazig University, in 2005. His Ph.D. thesis is entitled "Manipulation of Genetic Information in Studying Plant Performance." He is currently working as a Professor of Genetics and Agricultural Genetic Engineering with the Faculty of Agriculture, Zagazig University. He has published 14 papers in bioinformatics.